SUBUNIT INTERACTIONS WITHIN BOX C/D sRNPs

Timothy William Janzen
Bachelor of Science, University of Lethbridge, 2006

A Thesis
Submitted to the School of Graduate Studies
of the University of Lethbridge
in Partial Fulfilment of the
Requirements for the Degree

MASTER OF SCIENCE

Department of Chemistry and Biochemistry
University of Lethbridge
LETHBRIDGE, ALBERTA, CANADA

Signature Page

ABSTRACT

Box C/D small ribonucleoproteins (box C/D sRNPs) are responsible for the 2'-*O*-methylation required for the complete maturation of precursor rRNA. Archaeal box C/D sRNPs, like eucarya, are composed of four components: a guide RNA (box C/D sRNA), an RNA binding protein (L7ae), a 2'-*O*-methyltransferase (Fibrillarin) and a structural protein (Nop5). Here we develop several approaches for studying box C/D sRNP assembly. In particular, we have used pulldown and mobility shift assays to identify box C/D sRNP assembly intermediates (Nop5-aFib and L7ae-sR1). We have also demonstrated that isothermal titration calorimetry (ITC) can be utilized to quantitatively characterize the energetics of formation for the L7ae-sRNA assembly intermediate.

ACKNOWLEDGMENTS

First and foremost, I would like to thank my family (Corrine, Bill, Dorothy, and Ken) for their endless support and encouragement.

To Dr. Steven Mosimann, I would like to express my great appreciation for the opportunity to learn and grow as a student in his laboratory. The experience and skill set that I have acquired will be of great use in any future endeavour.

I would also like to thank my committee members, Dr. Hans-Joachim Wieden and Dr. David Siminovitch for their support and guidance throughout my time at the University of Lethbridge.

I am very grateful for the financial support I have received from the University of Lethbridge and the province of Alberta.

Last, but not least, I would like to thank my many colleagues from the Mosimann laboratory for their friendship and contributions to the following work.

TABLE OF CONTENTS

LIST OF FIGURES

LIST OF TABLES

LIST OF EQUATIONS

LIST OF ABBREVIATIONS

AdoMet	s-adenosylmethionine
BME	β-mecaptoethanol
BSA	bovine serum albumin
CD	circular dichroism
DNA	deoxyribonucleic acid
DNase	deoxyribonuclease
DTT	dithiothreitol
EDTA	Ethylenediaminetetraacetic acid
EMSA	electrophoretic mobility shift assay
FRET	fluorescence resonance energy transfer
GAR	glycine arginine rich
GMP	guanosine monophosphate
IMAC	immobilized metal-ion affinity chromatography
iPPase	inorganic pyrophosphatase
IPTG	isopropyl-beta-D-thiogalactopyranoside
ITC	isothermal titration calorimetry
k-turn	kink-turn
K_d	dissociation constant
LB	luria-bertani
mRNA	messenger ribonucleic acid
NTP	nucleoside triphosphate
RNP	ribonucleoprotein
RNA	ribonucleic acid
PCR	polymerase chain reaction
PMSF	phenol methyl sulfonyl flouride
RNase	ribonuclease
rRNA	riborsomal ribonucleic acid
SDS	sodium dodecyl sulfate
SDS-PAGE	sodium dodecyl sulfate polyacrylamide gel electrophoresis
SEC	size exclusion chromatography
sRNP	small ribonucleoprotein
snoRNA	small nucleolar ribonucleic acid
snoRNP	small nucleolar ribonucleoprotein
sRNA	small ribonucleic acid
TAE	tris acetate EDTA
T_m	melting temperature
Tris-HCl	2-amino-2-(hydroxymethyl)-1,3-propanediol, hydrochloride
tRNA	transfer ribonucleic acid

CHAPTER 1: OVERVIEW

1.1 Ribonucleoproteins

Ribonucleoproteins (RNPs) are macromolecular complexes composed of ribonucleic acid (RNA) and protein subunits. RNP particles are present in all branches of life and are divided into many classes, including heterogeneous nuclear ribonucleoproteins (eg. transcription complexes), cellular production machinery (eg. ribosome), small RNPs (sRNPs) (eg. Box C/D and H/ACA sRNPs), signal recognition particles (eg. protein coated ribozyme), and reverse transcriptases (eg. telomerase) (Wassarman *et al.* 1999; Eddy 2001; Erdmann *et al.* 2001; Omer *et al.* 2003). The two main classes of nucleotide modification complexes in archaea share common core RNP elements that likely evolved from a progenitor RNP (Tran *et al.* 2004). The presence of these core RNP elements in the ribosome suggests that the progenitor RNP may in fact lie in the primitive translation apparatus, and that the modern RNP world may have evolved from translational RNP elements during the transition from the ancient to modern RNP worlds (Tran *et al*. 2004). Originally, small nucleolar RNPs (snoRNPs) were identified and characterized only in eucaryotic cells, but more recently homologous RNP complexes (sRNPs) have been found to exist in archaea as well (Omer *et al.* 2003). Even the viral RNA-dependent RNA polymerases (eg. Polio virus) can also be classified as RNPs because they contain both protein and RNA components (Beattie *et al.* 2001; Brosius 2005). The high prevalence of these macromolecules in all organisms suggests they play a crucial role in cell viability and warrant further investigation.

In general, RNPs have a large but varying number of components and highly dynamic structures (Omer *et al.* 2003). For example, telomerases (Beattie *et al.* 2001)

and spliceosomes (Kiss 2004) have been shown to adopt multiple conformations to modulate recognition and processivity. The ribosome, which is crucial for cell viability, adopts several well documented conformations during catalysis (Voet and Voet 2004). A typical bacterial cell contains more than 15,000 ribosomes at any given time and ribosome assembly requires the coordination of 4 RNA molecules and roughly 50 different protein components (Fallon *et al.* 1979). The fully assembled ribosome always contains the same protein and RNA components, resulting in the same quaternary structure. This structure suggests a strictly monitored assembly mechanism to ensure a functional particle is constructed. Since all RNPs must form correctly, assembly information obtained from the smaller complexes can provide insight into how the larger, more complex RNPs form a functional particle as well.

1.2 Cellular modification of RNAs

The rRNAs and tRNAs of all organisms undergo many post transcriptional modifications around regions of key translational importance (Fatica and Tollervey 2003). The two most common types of RNA modification in both eucarya and archaea are the methylation of the ribose 2'-hydroxyl (2'-*O*-methylation) and the conversion of uridine to pseudouridine (Ψ) by base rotation (Reichow *et al.* 2007). Both of these modifications are directed by small guide RNAs known as small nucleolar RNAs (snoRNAs) in eucarya and sno-like RNAs (sRNAs) in archaea, as they do not contain a true nucleolus (Fatica and Tollervey 2003). In archaea, these sRNAs direct the modification of both the rRNA and tRNA, but the eucaryal counterparts only modify rRNA and have evolved separate enzymes for modifying tRNA (Clouet d'Orval *et al.* 2001).

The modification of RNA molecules is thought to facilitate both the folding and stability of rRNA (Kiss-Laszlo et al. 1996; Kiss-Laszlo et al. 1998). Modification by 2'-*O*-methylation of RNAs can protect the molecule from degradation by RNases and acid/base hydrolysis, both of which require the ribose 2'-hydroxyl for catalysis (Kowalak *et al.* 1994). Additionally, it has been suggested that the methylation complex may function as chaperone, pairing with nascent rRNA during assembly and directing localized RNA folding (Bachellerie *et al.* 1995; Dennis *et al.* 2001). This could function to prevent the formation of non-productive RNA structures which may interfere with downstream functions (Maxwell and Fournier 1995). This is supported by methylation patterns identified in extreme thermophiles, which appear to have a broader distribution and higher ratio of modified bases, possibly reflecting the more stringent need for stabilizing factors (Dennis *et al.* 2001; Omer *et al.* 2003).

Deletion of either single or multiple genes encoding for box C/D guide RNAs has little to no detectable phenotype, suggesting that in the absence of a few modifications downstream RNA function is not impeded (Lowe and Eddy 1999). In contrast, Tollervey *et al.* (1991) demonstrated that abolishing methylation activity completely has a significant impact on cell viability. In this work, they depleted Fibrillarin by placing it under expression control of a GAL promoter (only expressed in the presence of galactose) and growing cells on glucose medium. As the Fibrillarin levels decreased, they found that cell growth was progressively impaired and the level of rRNA and cytoplasmic ribosomes was reduced. In addition to methylation content, a high specificity for the target site is also crucial because modification of incorrect RNA bases can lead to toxicity by impacting downstream RNA function (Liu *et al.* 2001). This

information suggests that accurate global RNA methylation is essential to cell viability and may provide a mechanism for controlling cell growth.

During ribosomal maturation, the precursor rRNA transcripts are modified by sRNPs at more than 200 (mammals) and 100 (yeast) conserved sites within the core regions (Omer et al. 2003). RNA modifying sRNPs (eg. box C/D sRNPs) are unusual because they do not always contain the same RNA component. Rather, each complex is assembled around one member from an entire family of RNAs and utilizes it as a guide to direct modification activity to a particular target (Hamma and Ferre-D'Amare 2004; Moore *et al.* 2004). This allows the same modification machinery to act on multiple targets, directed by the bound guide RNA molecule (Omer *et al.* 2003). Interestingly, these guide RNAs and conserved target sites for RNA modification have been identified in both eucaryotes and archaea (Gaspin *et al.* 2000; Omer *et al.* 2000). Additionally, homologous sRNP core protein components have also been identified, suggesting that RNA-guided nucleotide modifications are an ancient mechanism, predating the divergence of eucarya and archaea (Omer *et al.* 2000; Tran *et al.* 2003). In order to determine how these molecular machines function, a complete dissection and analysis of the component parts and how they assemble into complexes *in vitro* is required (Omer *et al.* 2003).

1.3 Structure and function of a complete archaeal box C/D sRNP

Eucaryotic box C/D methylation complexes consist of Fibrillarin (the catalytic methyl transferase), Nop56, Nop58 (gene duplication), and a 15.5kDa protein (Galardi *et al.* 2002; Kiss 2004), however these eucaryotic complexes were found to be transient and unstable, making them difficult to work with (Omer *et al.* 2003). Alternatively, archaea (prokaryotes distinct from bacteria) are believed to be closely related to the earliest eucaryotes and present a possible alternative to studying eucaryotic systems (Omer *et al.* 2002). These homologous subunits appear to interact and function similarly and present sequence identities of 45% for Fibrillarin, 33% for L7ae and 32% for Nop5 (human vs *Sulfolobus acidocaldarius*) (Omer *et al.* 2000). The thermophillic archaeal systems offer simpler alternatives to addressing structural and biochemical issues, as their protein complexes can be more easily produced and harvested from bacteria and have a higher likelihood to be sufficiently stable to retain function *in vitro* following reconstitution procedures (Omer *et al.* 2003).

The first evidence suggesting methylation of archaeal RNAs being RNA mediated came from biochemical studies with *Sulfolobus* (Omer *et al.* 2000). In this work, Omer *et al.* (2000) utilized antibodies against the aFib and Nop5 proteins to immunoprecipitate complexes from cell extracts. cDNA clones generated from the co-immunoprecipitated RNAs were found to contain well-defined C and D box consensus elements and recognizable internal C' and D' motifs. These RNAs were then confirmed to possess antisense sequences complementary to rRNA, and methyl modification was demonstrated using primer extension pause reactions. Omer *et al.* (2000) went on to demonstrate that these guide sRNAs can be identified in both of the main archaeal phyla (crenarchaeota

and euryarchaeota). The above immunoprecipitated archaeal sRNP complexes were further analyzed using western blot and sodium dodecylsulfate (SDS-PAGE) gels (Omer *et al.* 2002). These gels showed the complexes to be composed of three unique proteins, rather than the four previously seen in eucarya. The core proteins in the archaeal sRNPs were identified as a Fibrillarin homolog (aFib), a single homolog to Nop56/Nop58 (Nop5) and a ribosomal protein homologous to the 15.5kDa protein (L7ae) (Fatica and Tollervey 2003). Table 1.1 below outlines the homologous components, and their function, between archaeal and eucaryal box C/D systems.

Table 1.1. Components of archaeal and eucaryal box C/D RNP complexes.

Archaeal system	Eucaryal homolog	Component function
sRNA	snoRNA	Guide RNA
aFibrillarin	Fibrillarin	2'-*O*-Methyltransferase
L7ae	15.5kDa protein	Box C/D RNA binding protein
Nop5	Nop56 and Nop58	Box C/D RNP structural protein

1.3.1 Fibrillarin is the catalytic subunit of the methylation complex

Structural information for Fibrillarin was obtained from the crystal structures from the euryarchaeons *Methanococcus jannaschii* (mjFib PBDID: 1FBN) (Wang *et al.* 2000), *Archaeoglobus fulgidus* (PBDID: 1NT2) (Aittaleb *et al.* 2003) and *Pyrococcus furiosus* (1PRY) (Deng *et al.* 2004). The structural features of these models all revealed the presence of 2 domains, C-terminal and N-terminal. The C-terminal domain was similar to previously seen catalytic methyltransferases domains, but the N-terminal domain presented a novel fold with unknown function (Wang et al. 2000).

The Fibrillarin N-terminal domain consists of a crescent-shaped, five-stranded β-sheet motif has varying length among Fibrillarin homologs (Wang *et al.* 2000).

Further, the mjFib crystal structure displayed two Fibrillarin molecules forming a dimer through their N-terminal domains, resulting in a buried surface area of 1700Å^2, well above the suggested dimerization value of 1050Å^2 (Chothia and Janin 1975). Additionally, when mjFib is run on non-denaturating polyacrylamide gel electrophoresis, it appears non-monomeric (Wang *et al.* 2000). Conversely, Fibrillarin homologues from *Archaeoglobus fulgidus* and *Pyrococcus furiosus*, which both have a shortened N-terminal domain, appear as monomers in their X-ray crystal structures and elute from gel filtration columns at volumes corresponding to monomers (Aittaleb *et al.* 2003; Deng *et al.* 2004). The longer N-terminal crescent-shaped β-sheet motifs present in some organisms (eg. mjFib and most crenarchaeota) may be able to assemble into more stable β-barrel structures in solution, resulting in a stable dimeric quaternary structure (Wang *et al.* 2000).

Experimentally, Fibrillarin homodimers have been detected by isothermal titration calorimetry (ITC), analytical ultracentrifugation and size exclusion chromatography (SEC) (Burke 2006). If the N-terminal domain was removed, no aFib dimers were detected by any of the methods, again suggesting the N-terminal domain is responsible for dimer formation. From the ITC measurements, the dissociation constant for the transition to a Fibrillarin monomer is 61.9μM (Burke 2006). When compared to overall cellular levels this value seems unreasonably high, however methylation complexes tend to be localized around centers of ribosome biogenesis. In fact, eucaryotic Fibrillarin is the most abundant nucleolar protein (Eichler and Craig 1994). This localization could potentially increase the local (effective) concentration of Fibrillarin high enough for

dimer formation. The existence of such a homodimer alludes to a possible alternative mode to assembling a fully functional archaeal sRNP particle.

The C-terminal domain of these models all revealed structural similarities to enzymes known to catalyze methyl transfer from a cofactor, *S*-adenosylmethionine (AdoMet), to a variety of substrates (eg. nucleic acids, proteins and small-molecule metabolites) (Cheng and Roberts 2001; Martin and McMillan 2002). The methyltransferase family displays little sequence identity, but does have common structural characteristics that can be identified in the Fibrillarin structures. Further, a structural comparison of Fibrillarin from archaea and eucarya (Wu *et al.* 2006) organisms demonstrates that with the exception of the eucaryal amino(N)-terminal glycine arginine rich (GAR) domain absent in archaea, they are structurally very similar (Reichow *et al.* 2007). This extended N-terminal domain, responsible for nucleolar localization in eucarya, is not necessary in archaea as they do not contain a true nucleolus (Heine *et al.* 1993).

Despite the low sequence identity, the carboxy(C)-terminal domain of Fibrillarin is structurally similar to the AdoMet binding in several methyltransferases enzymes. The root-mean-squared deviation of 49 backbone Cα positions varies from 1.3Å to 2.1Å, which is lower than expected for a conserved motif (Wang *et al.* 2000). Further, Wang was able to identify the short "AdoMet binding motif" consensus sequence in the C-terminal domain and predict the likely residues involved in binding. In order to experimentally confirm the predicted AdoMet binding site, Omer *et al.* (2002) made two amino acid substitutions (A85V and P129V) in the proposed binding pocket of Fibrillarin from *Sulfolobus solfataricus*. In both cases RNPs complexes of the expected molecular

weight were assembled, but were found to be either partially or completely unable to catalyze methyl transfer to RNA. This data confirms the role of the Fibrillarin C-terminal domain and suggests that RNP assembly is not dependent on AdoMet binding. Rather, AdoMet binding is only required during the catalytic methyl transfer step.

1.3.2 Nop5

There currently exists no structure of Nop5 as a single species. However, in 2003 Aittaleb *et al.* was able determine the crystal structure of Nop5 in complex with Fibrillarin from *Archaeoglobus fulgidus* (PBDID: 1NT2). This model revealed Nop5 to have two domains (N and C-terminal) connected by a long coiled-coil region, a classic protein motif that is often involved in oligomerization (Kohn *et al.* 1997; Burkhard *et al.* 2001). The N-terminal domain contains an exposed hydrophobic surface that is responsible for mediating interactions with Fibrillarin, while the C-terminal domain contains a structural fold similar to RNA binding domains which is observed in all of the Nop family proteins (Hardin et al. 2009). Nop56/58 is well conserved (eg. 52% identity between human and yeast Nop56), however eucaryotic homologs (eg. yeast) do contain an additional small KKE/D motif (microtubule binding motif) in their C-terminal domain not present in the Nop5 of archaea (Gautier *et al.* 1997). Deletion of this motif (Gautier *et al.* 1997) does not impair cell viability, suggesting it is not directly involved in sRNP assembly or catalysis and is more likely to be a localization signal that is not necessary in archaea.

The model presented by Aittaleb *et al.* (2003) illustrated a coiled-coil mediated dimer with a buried surface area of 2868Å^2, again suggesting a stable interaction *in vivo*. Additionally, Oruganti *et al*. (2007) present a crystal structure of this same complex from

Pyrococcus furiosus which also illustrates a strong Nop5 homodimer mediated by the coiled-coil domain. When they compared this crystal structure to the previous model from *A. fulgidus* (Aittaleb *et al.* 2003) they discovered that the Nop5 domains had the same overall structure, but were positioned with different orientations. A block normal mode analysis of these two structures indicated that the two observed conformational states can be interchanged by hinge motions of least energy cost (Oruganti *et al.* 2007).

In 2006, Zhang *et al.* investigated the role of the coiled-coil domain in Nop5 by creating truncation mutants of Nop5 that removed the coiled-coil region. With these mutants they were still able to assemble sRNP particles of the expected size, but these alternative complexes were completely devoid of methylation activity. This data suggests that the coiled-coil domains may not be required for initial sRNP assembly, but plays some role in the later stages of catalysis. One possibility is a post-assembly restructuring event (mediated by the coiled-coil domains) that could be required to reposition the catalytic Fibrillarin subunits over the target methylation site (Zhang et al. 2006; Ye et al. 2009). The two static structures determined by Oruganti *et al.* (2007) and Aittaleb *et al.* (2003) may actually represent the two most stable conformations of a highly dynamic complex.

1.3.3 Box C/D sRNAs

The RNAs responsible for directing archaeal ribose 2'-*O*-methylation are termed box C/D sRNAs and contain a conserved box C (RUGAUGA, where R stands for any purine) and box D (CUGA) motif near the 5' and 3' ends respectively (Kiss 2001; Omer *et al.* 2003). Most archaeal guide sRNAs are bipartite, containing a second, degenerate box C/D (termed C'/D'), in addition to the one or two regions of complementarity to

target RNAs (Bachellerie *et al.* 1995; Tran *et al.* 2005). This information suggests that a single guide sRNA can potentially direct the methylation of two target sequences simultaneously (Tran *et al.* 2003). In contrast, the eucaryotic guide RNAs tend to be longer than the archaeal counterparts (75-100nt versus 50-60nt) and are predominantly monopartite (Omer *et al.* 2000). By using guide RNAs to direct methylation to a particular target sequence, a single RNP particle can potentially catalyze the methylation of any target RNA, providing a complementary guide exists. The nucleotide targeted for 2'-*O*-methylation is determined by the "N plus five" rule, which dictates that the nucleotide paired to the guide RNA precisely 5bp upstream of the D or D' box of the sRNA is modified (Kiss-Laszlo et al. 1996; Tycowski et al. 1996; Kiss-Laszlo et al. 1998).

In solution, RNA molecules contain various levels of secondary structural motifs (Shen *et al.* 1995). The box C/D sRNAs contain a conserved protein-binding sequence known as the kink-turn (k-turn) motif, originally identified by examination of crystal structures of the ribosomal subunits (Klein *et al.* 2001; Omer *et al.* 2003). Most identified k-turn RNAs are involved in protein binding, suggesting the conformation is an important recognition element (Goody *et al.* 2004). As illustrated in Figure 1.1 below, this structure is characterized by a kink in the phosphodiester backbone that bends the RNA helix axis by approximately 120°. Further, this helix kink contains two sheared base pairs, and causes a nucleotide (in this case Uracil 27) to protrude from the structure and become accessible for protein binding. This protruding nucleotide is critical for the binding interaction between proteins and the RNA molecule (Reichow *et al.* 2007). Goody *et al.* (2004) used polyacrylamide gel electrophoresis to investigate the need for

sheared base pairing in the k-turn region and showed that the presence of kinks would cause RNA molecules to migrate through the gels at a slower rate (retarded mobility). Further, any deviation from the G-A pairings reduces mobility retardation nearly completely (Goody *et al.* 2004) and impedes protein binding interactions (Rozhdestvensky *et al.* 2003), indicative of a k-turn free structure. This data suggests that these unusual base pairings are critical for the successful formation of a k-turn.

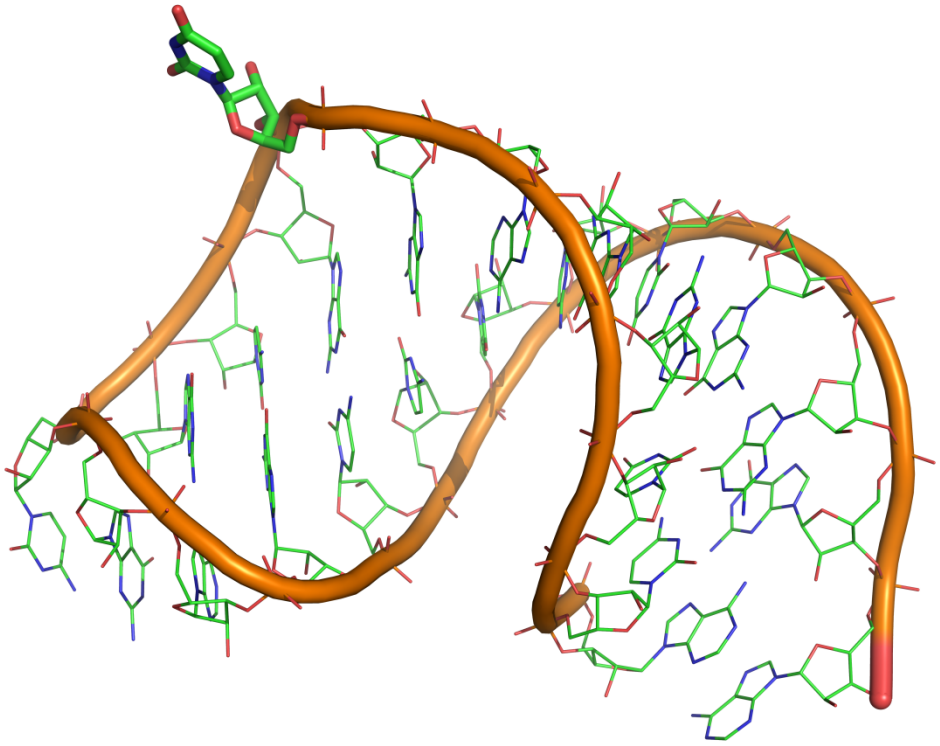

Figure 1.1. A cartoon model illustrating the RNA kink-turn motif. The non-canonical base pairing and nucleotide bulge between stem I and stem II cause an approximate 120° kink in the RNA backbone. As can be seen, this kink causes nucleotide U27 to protrude and become accessible for protein binding.

Fluorescence resonance energy transfer (FRET) (Goody *et al.* 2004; Suryadi *et al.* 2005) and circular dichroism (CD) (Gagnon *et al.* 2006) studies of k-turn sRNAs demonstrate that the formation of tightly kinked conformations, as seen in the crystal structures (Hamma and Ferre-D'Amare 2004; Moore *et al.* 2004), may in fact be only

transiently sampled by free RNA. Further, it has been shown (Goody *et al.* 2004) that the k-turn structure is only stably formed when either complexed with protein or in the presence of large amounts of divalent cations. They demonstrate that the bulge created by the k-turn in the presence of 5mM magnesium ions would greatly retard migration during polyacrylamide gel electrophoresis. Additionally, if either 2mM EDTA was substituted for magnesium, or the k-turn motif was mutationally disrupted, the retarding effect was minimized. This data suggests that divalent magnesium ions are also playing a critical role in stabilizing the k-turn motif.

To further investigate the effect of magnesium on k-turn formation, Goody *et al.* (2004) fluorescently labelled the two ends of the RNA molecule (sR8). With this approach the formation of a k-turn motif, bringing the two ends together as seen in Figure 1.1 above, would be accompanied by an increase in FRET efficiency. Using this assay Goody *et al.* (2004) again showed that magnesium ions induced a more tightly kinked structure. More interestingly, they found that the addition of sodium ions induced a similar conformational change. They calculated the 50% transition state to occur at 1mM (magnesium ions) or 72mM (sodium ions) (Goody *et al.* 2004), however even at relatively high concentrations the extended (non k-turn) conformation was present in significant amounts. Moreover, the sR8 C/D and C'/D' boxes have less sequence variation from the box C/D consensus sequences than most other guide sRNAs, possibly presenting a best case scenario for k-turn formation. This information suggests that under physiological conditions, it is likely that some or all of the k-turn structures require stabilization. The above data all leads to the conclusion that the k-turn motifs previously

identified in the crystal structures do actually occur in solution, but are much more dynamic than originally thought (Goody *et al.* 2004).

1.3.4 L7ae

L7ae is known to play at least three roles in archaeal organisms (Box C/D and H/ACA sRNPs and functions as a ribosomal protein), suggesting it may enable cells to coordinate rRNA processing and ribosome assembly (Tran *et al.* 2003). This protein has a small (~14 kDa) single domain structure composed of a central four-stranded β-sheet sandwiched between twelve α-helices (six on each side) (Moore et al. 2004). In contrast to the highly dynamic RNA structures in solution, the L7ae structure was found to be nearly identical in the RNA-bound (PDBID: 1SDS and 1RLG) (Hamma and Ferre-D'Amare 2004; Moore *et al.* 2004) and RNA-free state (PDBID: 1XBI and 1RA4) (Suryadi *et al.* 2005). Using circular dichroism Suryadi *et al.* (2005) was able to demonstrate that L7ae can induce structural changes in the box C/D and C'/D' regions, similar to the effects described above when titrating the sR8 RNA with magnesium. *In vitro* reconstitution of archaeal box C/D sRNP particles demonstrated that L7ae is required for initiating RNP assembly at the conserved box C/D and C'/D' motifs of the guide sRNAs (Omer *et al.* 2002).

L7ae is part of an RNA-binding protein family that recognizes the conserved k-turn motifs found in the guide sRNAs (Rozhdestvensky *et al.* 2003; Moore *et al.* 2004). Members of this family were originally all thought to recognize the k-turn motif through the conserved αβα sandwich motif described previously. In the case of L7ae, the steric hindrance and specific amino acid contacts in this sandwich motif limit the protein to binding an extruding U nucleotide only (Klein *et al.* 2001). The protein then encases the

U nucleotide in a hydrophobic pocket to stabilize base-specific hydrogen bonding interactions (Moore *et al.* 2004). These observations suggest that L7ae may act as a fixed scaffold, initiating complex assembly by selecting and stabilizing the appropriately folded guide sRNAs in solution (Moore et al. 2004). More recently however, a eucaryotic L7ae homolog (NHP2) has been shown to bind H/ACA sRNAs by an alternative non k-turn specific interaction (Ofengand 2002; Wang and Meier 2004), suggesting that alternative assembly modes are also possible.

1.4 Assembling an archaeal box C/D sRNP

The interactions between box C/D sRNP components have been investigated many ways including: immunoprecipitation (Omer *et al.* 2000; Omer *et al.* 2002), tandem affinity purification and mass spectrometry (Galardi *et al.* 2002), electrophoretic mobility shift assay (Rozhdestvensky *et al.* 2003; Gagnon *et al.* 2006; Zhang *et al.* 2006), calorimetry (Aittaleb *et al.* 2004), and crystal structures (Wang *et al.* 2000; Aittaleb *et al.* 2003; Deng *et al.* 2004; Moore *et al.* 2004; Suryadi *et al.* 2005; Oruganti *et al.* 2007; Hardin *et al.* 2009). These experimental approaches have been used on samples from a wide variety of organisms (both eucaryotic and archaeal). Overall, the data obtained from using the various techniques above yield similar information regarding inter subunit interactions.

Using the components identified by immunoprecipitation L7ae, Nop5, and aFib have been shown to form identical, symmetric complexes at both the box C/D and C'/D' motifs, as illustrated in Figure 1.2 below (Tran *et al.* 2003). *In vitro* gel retardation studies using recombinant Fibrillarin and a box C/D RNA transcript show that neither Fibrillarin, nor Nop5, nor a combination of Fibrillarin and Nop5 are able to interact with

the RNA molecule (Omer *et al.* 2002). Additionally, they found that if L7ae is pre-bound to the RNA first, the addition of Nop5 (but not Fibrillarin) would create a higher retarding force (suggesting a larger molecular weight complex was formed). Subsequently incubating Fibrillarin with the pre-assembled L7ae-sRNA-Nop5 generated an even larger molecular weight complex (presumably the fully assembled complex) (Omer *et al.* 2002). This stepwise mechanism to complex assembly is similar to that proposed by Nottrot *et al.* (2002) for the human U4/U6 sRNP complex (the 15.5kDa protein binds to RNA followed by the remaining components associating independently of each other), but does not eliminate the possibility that Nop5 and Fibrillarin assembling into the box C/D complex as a pre-formed heterodimer (Ye *et al*. 2009).

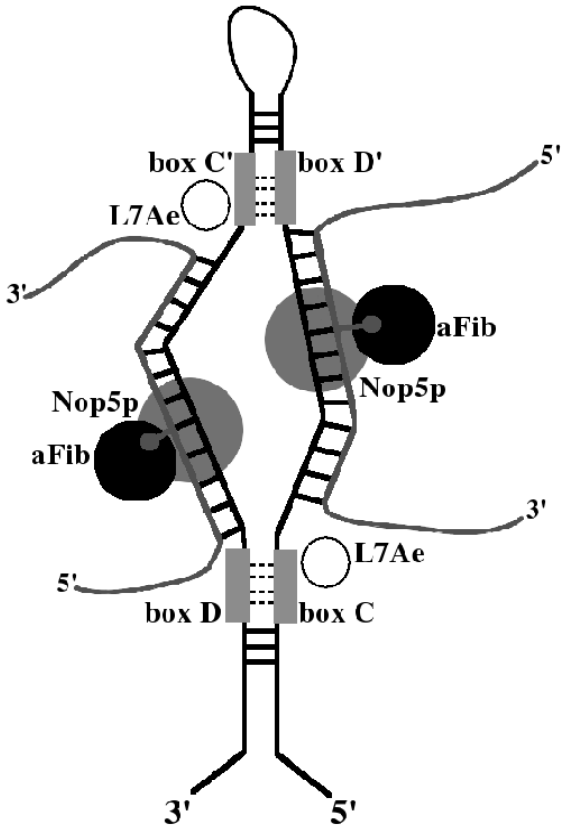

Figure 1.2. A cartoon diagram (Burke 2006) demonstrating the minimal box C/D sRNP from archaea with the box C/D and C'/D' motifs illustrated by gray boxes. The target RNA is duplexed with the guide and methyl groups are indicated by circles. Note that protein and RNA components are not drawn to scale.

It has been proposed that a single target RNA molecule with two regions complementary to the guide sRNA may base pair with both the box C/D and C'/D' guides to methylate two separate yet closely positioned nucleotides of the same target, however, it is also possible that only one of the above described sites is modified, while the other site of complementarity is used for stabilizing the complex (Omer *et al.* 2003). Efficient methylation requires that both the terminal C/D and internal C'/D' RNP complexes function together (Tran *et al.* 2003). Evidence from Bortolin *et al.* (2003) and Omer *et al.* (2006) demonstrate that the cooperative interactions between these two complexes are critical for catalysis. They showed that when the box C/D or C'/D' k-turn

motifs were disrupted mutationally, preventing complex assembly at one site, the methylation efficiency is adversely affected *in vitro*. This data indicates that a dimer of heterotrimers must exist on the guide RNA molecule, even if only one target methylation site is present.

1.4.1 Fibrillarin interacts with Nop5

Crystal structures containing archaeal Nop5 and Fibrillarin consistently show extensive contacts between the two polypeptide chains. In addition, the Nop5-Fibrillarin complexes form heterotetramers or dimers of the Nop5-Fibrillarin complex. In all cases, the dimeric interaction between these complexes is mediated by Nop5 (Aittaleb *et al*. 2003; Aittaleb *et al*. 2004; Oruganti *et al*. 2007). The N-terminal domain of Nop5 is unstable and Aittaleb *et al.* (2003) suggest that it is likely not an autonomously folding unit and is primarily stabilized though interactions with Fibrillarin. The Nop5-Fibrillarin interface buries a large region (2637Å^2) of the solvent accessible surface area, indicative of a stable interaction (Aittaleb *et al.* 2003). Interestingly, this surface area is predominately nonpolar, and suggests that this interaction is not dictated by a single amino acid but rather an overall surface complementarity (Aittaleb *et al.* 2003). Further, only two pairs of contact residues between Fibrillarin and Nop5 involve side chain interactions while the remaining interactions are formed through main chain contacts. This information again indicates that a surface geometric complementarity is more important than sequence identity, as the convex surface of Fibrillarin easily fits into the concave N-terminal domain of Nop5 to form a stable interaction (Aittaleb *et al*. 2003).

The Fibrillarin/Nop5 heterodimers appear to further dimerize through a four-helix bundle formed by the coiled-coil domains of Nop5 (Figure 1.3). The resulting complex is

a 111.7kDa tetramer that is consistent in size with fractions obtained by gel filtration chromatography (Aittaleb *et al.* 2003). This large quaternary structure represents one possible assembly mode to position the catalytic Fibrillarins over their target nucleotides and coordinate the activity between the two methylation sites. Interestingly, the different structures of the Nop5-Fibrillarin complex show varying domain orientations (Oruganti *et al.* 2007). This structural information suggests that these intermediates represent a highly dynamic complex that may rotate freely about a Nop5 N-terminal domain hinge, becoming locked in a final, active conformation upon binding substrate RNA.

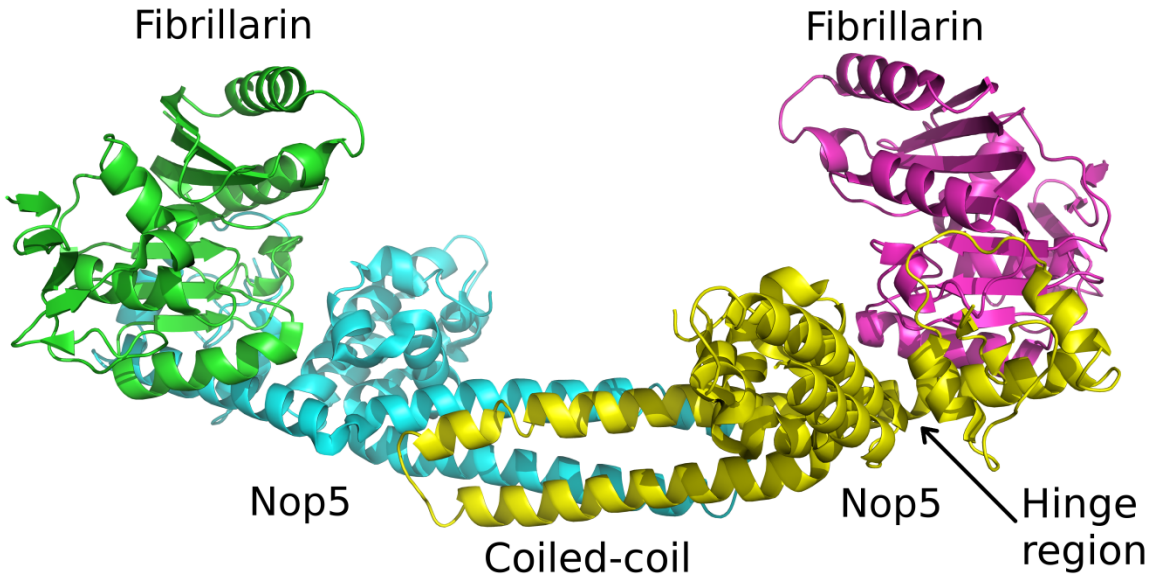

Figure 1.3. A crystal structure of the *A. fulgidus* Nop5-Fibrillarin tetrameric complex, illustrating the coiled coil domains of Nop5 forming a bridge between the two Nop5 Fibrillarin heterodimers.

In vivo experiments (Lechertier *et al.* 2009) show that neither the RNA biding domain, nor the eucaryal GAR domain are involved in Nop56/58-Fibrillarin heterodimer formation. These experiments confirm that the eucaryotic components behave largely the same as their archaeal counterparts with the exception of Nop58 (not present in archaea)

which appears to respond differently to Fibrillarin than Nop56. This data agrees with the previous models whereby biogenesis is mediated by dynamic multisubunit complexes that coordinate RNP assembly, localization and processing events, but suggests that we do not fully understand the differences between Nop56 and Nop58.

1.4.2 Assembling a complete sRNP particle

As described above, there is strong evidence for both the Nop5-Fibrillarin and L7ae-sRNA intermediate complexes. Additionally, the recent work of Hardin *et al.* (2009) demonstrates that the C-terminal domain of Nop5 (Nop domain) forms stable interactions with the L7ae-sRNA complex (K_d 106nM). Further, Tran *et al*. (2003) showed that Fibrillarin enhances the binding of Nop5 to the L7ae-RNA, suggesting it does in fact preferentially bind as a preformed Nop5-Fibrillarin heterodimer. Hinge movements between the dimeric Nop5 and Fibrillarin could then position one catalytic copy at each methylation target site. In this model (Figure 1.4), the Fibrillarin-Nop5 dimer (or tetramer) is recruited by the L7ae-sRNA complex.

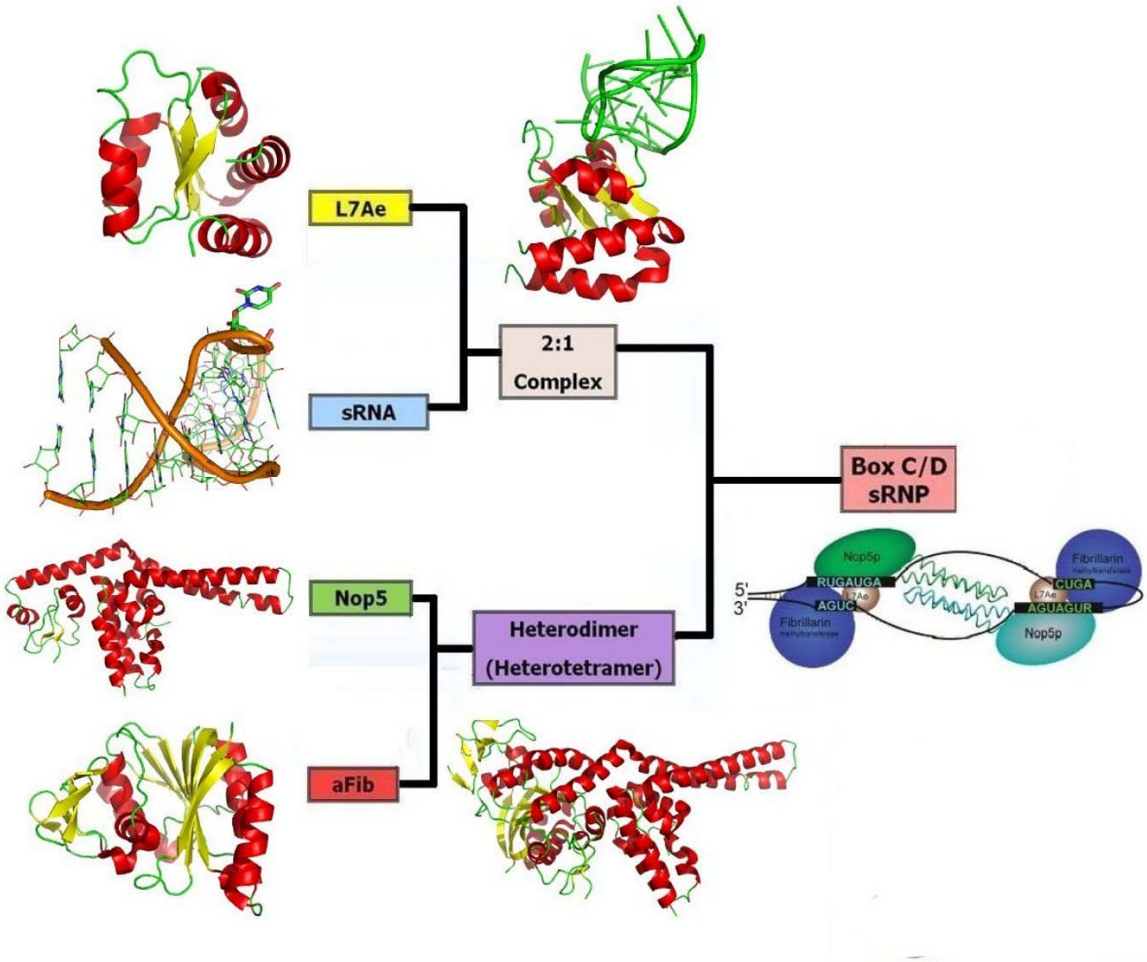

Figure 1.4. A cartoon diagram illustrating the most likely pathway to assemble an archaeal sRNP particle. L7ae/RNA and Nop5/Fibrillarin form intermediate complexes which then interact to form a complete box C/D sRNP.

A completely assembled box C/D sRNP particle can be modeled by positioning the crystal structures from the components into the proposed model illustrated on the right side of Figure 1.4. This model agrees with virtually all experimental data collected however, it positions the two Fibrillarin active sites approximately 80Å apart, much further than the 25-35Å distance between the box C/D and C'/D' motifs (Oruganti *et al.* 2007; Reichow *et al.* 2007). The distance cannot be accommodated by a rigid adoption of the model and presents a significant problem because it incorrectly positions the Fibrillarin active sites for methylation. Zhang *et al*. (2006) suggested that the coiled-coil

domains of Nop5 may allow for a critical restructuring event to occur post assembly to activate the particle. This restructuring event could account for the 2 different structures seen by Oruganti *et al.* (2007) and also adopt a conformation with a shorter distance between the two Fibrillarin active sites. Upon complete assembly, the target RNA can base pair with the guide sequence and the coiled-coils of Nop5 can further mediate the cooperativity between the C/D and C'/D' sites through possible hinge motions positioning Fibrillarin over each methylation target (Oruganti *et al.* 2007). At this time, methylation occurs and the target sRNA can be released in its modified state. The dynamic flexibility of this system presents the possibility of an intermediate restructuring event repositioning the complex over the second methylation target (Oruganti *et al.* 2007). In this work we investigate the subunit interactions within an archaeal box C/D methylation sRNP complex from the archaeon *Sulfolobus solfataricus* and propose an additional intermediate complex may also form *in vivo*.

CHAPTER 2: MATERIALS AND METHODS

2.1 Buffers and Reagents

The following is a list of all the buffers and reagents used in the methods described below.

2.1.1 Detection Techniques

Acrylamide Solution (30% (w/v))

29g		Acrylamide
1g		Bis-acrylamide

Dilute to 100mL with deionized H_2O

SDS-PAGE Resolving Gel Premix (12% (w/v))

4.0mL	30% (w/v)	Acrylamide Solution
2.5mL	1.5M	2-amino-2-(hydroxymethyl)-1,3-propanediol,hydrochloride (Tris-HCl) (pH8.8)
0.1mL	10% (w/v)	Sodium dodecyl sulfate (SDS)
3.4mL		Deionized H_2O

SDS-PAGE Resolving Gel Premix (15% (w/v))

5.0mL	30% (w/v)	Acrylamide Solution
2.5mL	1.5M	Tris-HCl (pH8.8)
0.1mL	10% (w/v)	SDS
2.4mL		Deionized H_2O

SDS-PAGE Stacking Gel Premix (5% (w/v))

0.65mL	30% (w/v)	Acrylamide Solution
1.25mL	1.5M	Tris-HCL (pH8.8)
0.05mL	10% (w/v)	SDS
3.05mL		Deionized H_2O

Urea/Acrylamide Gel Premix (15% (w/v))

4.8g		Urea
5.625mL	30% (w/v)	Acrylamide Solution
40.0µL	0.5M	Ethylenediaminetetraacetic acid (EDTA) (pH8.0)
200.0µL	50x	Tris-acetate-EDTA (TAE)
1.875mL		Deionized H_2O

Native RNA PAGE Solution (15% (w/v))

5.0mL	30% (w/v)	Acrylamide Solution
200µL	50x	TAE
4.8mL		Deionized H_2O

Tris-Glycine Buffer (1x)

14.4g		Glycine
3.0g		Tris
1.0g		SDS

Dilute to 1L with deionized H_2O

SDS-PAGE Loading Buffer (2x)

1.80mL	100% (v/v)	Glycerol
2.16mL	0.5M	Tris-HCl (pH6.8)
4.00mL	10% (w/v)	SDS
1.00mL		β-mercaptoethanol (BME)
1.00mL	0.1% (w/v)	Bromophenol blue

SDS-PAGE Staining Solution

40% (v/v)	Methanol
10% (v/v)	Acetic acid
50% (v/v)	Deionized H_2O
0.25% (w/v)	Coomassie brilliant Blue R250

SDS-PAGE Destaining Solution

40% (v/v)	Methanol
10% (v/v)	Acetic acid
50% (v/v)	Deionized H_2O

TAE Buffer (50x)

242g		Tris-HCl
57.1mL		Glacial acetic acid
100mL	0.5M	EDTA (pH8.0)

Dilute to 1L with deionized H_2O

Agarose Gel Loading Buffer (Blue Juice)

1.6mL	0.25M	EDTA (pH8.0)
1.0mL	20% (w/v)	Sarkosyl
10mg		Bromophenol blue
3.0mL	100% (v/v)	Glycerol

Dilute to 20mL with deionized H_2O

Urea PAGE Loading Buffer

0.48g		Urea
200µL	100% (v/v)	Glycerol
100µL	0.1% (w/v)	Bromophenol blue

Dilute to 1mL with deionized H_2O

Urea PAGE Staining Solution
0.5% (v/v) Ethidium bromide in deionized H_20

Urea PAGE Destaining Solution
Deionized H_20

2.1.2 L7ae Purification

Buffer A	**L7ae Lysis/storage buffer**
10mM	Tris-HCl (pH 8.0)
100mM	NaCl
1mM	BME

Buffer B	**L7ae Immobilized Metal Affinity Chromatography rinse buffer**
10mM	Tris-HCl (pH 8.0)
100mM	NaCl
1mM	BME
0.1mM	EDTA
25mM	Imidazole (pH 8.0)

Buffer C	**L7ae IMAC elution buffer**
10mM	Tris-HCl (pH8.0)
100mM	NaCl
1mM	BME
0.1mM	EDTA
400mM	Imidazole (pH 8.0)

2.1.3 aFib Purification

Buffer D	**aFib Lysis buffer**
10mM	Tris-HCl (pH 8.0)
100mM	NaCl
1mM	BME
0.1mM	EDTA

Buffer E	**aFib Storage/SEC buffer**
10mM	Tris-HCl (pH 8.0)
100mM	NaCl
1mM	BME

Buffer F	**His-tagged aFib IMAC equilibration buffer**
10mM	Tris-HCl (pH 8.0)
100mM	NaCl
20% (v/v)	Glycerol
4.0M	Urea

Buffer G	**His-tagged aFib rinse buffer**
10mM	Tris-HCl (pH 8.0)
100mM	NaCl
20% (v/v)	Glycerol
4.0M	Urea
25mM	Imidazole (pH 8.0)

Buffer H	**His-tagged aFib elution buffer**
10mM	Tris-HCl (pH 8.0)
100mM	NaCl
20% (v/v)	Glycerol
4.0M	Urea
400mM	Imidazole (pH 8.0)

2.1.4 Nop5 Purification

Buffer I	**Nop5 IMAC equilibration and storage buffer**
50mM	Tris-HCl (pH 8.0)
400mM	NaCl
8.0M	Urea

Buffer J	**Nop5 IMAC rinse buffer**
50mM	Tris-HCl (pH 8.0)
400mM	NaCl
8.0M	Urea
25mM	Imidazole (pH 8.0)

Buffer K	**Nop5 IMAC elution buffer**
50mM	Tris-HCl (pH 8.0)
400mM	NaCl
8.0M	Urea
400mM	Imidazole (pH 8.0)

2.1.5 T7-Polymerase Purification

Buffer L	**T7-Polymerase IMAC equilibration buffer**
50mM	Tris-HCl (pH 8.0)
100mM	NaCl
1mM	BME
1mM	Imidazole
1mM	Phenol methyl sulfonyl fluoride (PMSF)
5% (v/v)	Glycerol

Buffer M	**T7-Polymerase IMAC rinse buffer**
50mM	Tris-HCl (pH 8.0)
100mM	NaCl
1mM	BME
10mM	Imidazole
5% (v/v)	Glycerol

Buffer N	**T7-Polymerase IMAC elution buffer**
50mM	Tris-HCl (pH 8.0)
100mM	NaCl
1mM	BME
100mM	Imidazole
5% (v/v)	Glycerol

Buffer O	**T7-Polymerase gel filtration buffer**
25mM	Tris-HCl (pH 7.5)
50mM	NaCl
1mM	EDTA
1mM	DTT

Buffer P	**T7-Polymerase storage buffer**
20mM	KH_2PO_4 (pH 7.5)
1mM	EDTA
1mM	DTT

2.1.6 Pulldown Assay

Buffer Q	**Pulldown assay Fibrillarin binding buffer**
10mM	Tris-HCl (pH 8.0)
100mM	NaCl
1mM	BME
25mM	Imidazole (pH 8.0)

Buffer R	**Pulldown assay elution buffer**
10mM	Tris-HCl (pH 8.0)
100mM	NaCl
1mM	BME
400mM	Imidazole (pH 8.0)
0.1M	EDTA

2.1.7 Isothermal Titration Calorimetry (ITC)

Buffer S	**ITC buffer 1**
50mM	Tris-HCl (pH 8.0)
250mM	NaCl
5mM	$MgCl_2$
Buffer T	**ITC buffer 2**
50mM	Tris-HCl (pH 8.0)
250mM	NaCl
2.5mM	$MgCl_2$

Buffer U	**ITC buffer 3**
50mM	Tris-HCl (pH 8.0)
83mM	$(NH_4)_2SO_4$
5mM	$MgCl_2$

2.2 Detection Techniques

2.2.1 SDS Polyacrylamide Gel Electrophoresis (SDS-PAGE)

SDS-PAGE gels were run as outlined by Laemmli in 1970. For visualizing aFib (28kDa) and L7ae (14kDa) the gels contained a 15% resolving gel, while for the larger Nop5 (56kDa) a 12% resolving gel was utilized. In both cases the gels contained a 5% stacking gel and were assembled into the Mini-Protean 3 gel apparatus (Biorad; Hercules, CA, USA). Protein samples were mixed with equal volumes of 2x SDS-PAGE loading buffer and incubated at 90°C for 5 minutes prior to loading. Both the inner and the outer reservoirs of the gel apparatus were filled with Tris-Glycine buffer and a voltage of 30V/cm was applied for 45-60 minutes at 20°C. Resulting gels were then incubated in the SDS-PAGE staining solution with gentle shaking for 15 minutes. Gels were then transferred to a SDS-PAGE destaining solution for 30 minutes before visualization with a white light transilluminator.

2.2.2 Agarose Gel Electrophoresis

Agarose gels were created by thermal dissolution of 0.4g of Agarose B (BioBasic; Markham, ON, Canada) in 40mL of TAE buffer to generate 1.0% agarose gels. Once the dissolved agarose had cooled to 40-45°C, ethidium bromide was added to a final concentration of 0.75% (v/v) and the mixture was then allowed to solidify in a Mini-Sub Cell GT Cell (Biorad). The gels were then immersed in 1x TAE buffer. DNA samples were complemented with an equal volume of agarose gel loading buffer immediately prior to loading. Gels were then run by applying a voltage of 6V/cm for 60-75 minutes at 20°C. Gels were visualized using an ultraviolet transilluminator (VWR) adjusted for 302nm emission.

2.2.3 Urea PAGE

Polymerized 15% Urea/Acrylamide gels were assembled in a Mini-protean 3 gel apparatus (Biorad) with the inner and outer reservoirs filled with pre-heated 1x TAE buffer (50-60°C). Prior to loading samples, the Urea/Acrylamide gels were also pre-heated by applying a 40V/cm voltage for 5 minutes. RNA samples were complemented with equal volumes of urea gel loading buffer and incubated at 90°C for 5minutes prior to loading. Loaded gels were then run at 40V/cm for 30-40 minutes at 20°C and subsequently immersed in a Urea PAGE staining solution for 15 minutes. Stained gels were then visualized with 302nm light using an ultraviolet transilluminator.

2.2.4 Protein Quantification

2.2.4.1 Absorbance at 280nm (A_{280})

For spectroscopic quantification, protein samples were denatured using 8M urea and the absorbance was measured at 280nm (adapted from Stoschek (1990)). An extinction coefficient for each molecule was predicted using the ExPASy server's ProtParam tool (Gasteiger *et al.* 2005) and concentration values were obtained using the Beer-Lambert equation. The predicted extinction coefficients are listed below in table 1.

Table 2.1. Predicted extinction coefficients used to quantify denatured proteins.

Molecule Measured	Extinction coefficient ($M^{-1}cm^{-1}$)
Nop5	$\varepsilon_{280} = 31860$
L7ae	$\varepsilon_{280} = 4595$
aFib	$\varepsilon_{280} = 29465$
aFib_n56	$\varepsilon_{280} = 17880$

2.2.4.2 Bradford Assay

Protein quantification using the Bradford approach requires a standard curve for the Bradford reagent (BioBasic) (Bradford 1976; Stoschek 1990). To generate the standard curve, 800µL protein solutions containing 0-10µg/mL bovine serum albumin (BSA) in the same buffer as the protein to be quantified were mixed with 200µL Bradford reagent. Protein samples to be quantified were then treated as described above and concentrations were determined by interpolation of the standard curve.

2.3 The expression and purification of protein components

2.3.1 Over expression and purification of L7ae

The L7ae gene sequence was previously cloned (Burke 2006) into the NheI restriction site of the pET28a^{Kan} expression vector (EMD Biosciences; San Diego, CA, USA) which contains a thrombin cleavable amino terminal 6x His tag. Aliquots of calcium chloride competent BL21 (DE3) strain *Escherichia coli* (*E. coli*) cells (prepared as described in Sambrook and Russell, (2001)) were individually transformed with the above vector using a 30 second heatshock, as outlined in Sambrook and Russell (2001). Resulting colonies were grown in 5mL Luria-Bertani (LB) broth at 37°C until an optical density of 0.5-0.7 at 600nm was reached and then induced using 1mM isopropyl-beta-D-thiogalactopyranoside (IPTG). Inoculated cells were then over expressed overnight with shaking at 37°C and screened for expression. Positive expressing clones were subsequently used in larger scale (1L) cell growths. Accumulated cells were pelleted at 5500x*g* for 20 minutes using an Allegra 25R centrifuge (Beckman Coulter; Fullerton, CA, USA). Pellets were then stored at -80°C until lysis.

Cells over expressing L7ae were lysed using a Sonic Dismembrator Model 100 (Fisher Scientific; Pittsburgh, PA, USA) in buffer A using three 30 second pulses, interspaced by 30 seconds on ice. The resulting lysate was then centrifuged at 21100x*g* for 1 hour at 4°C. L7ae was then purified from the cell lysate using a 5mL Ni-NTA agarose column (Qiagen; Hilden, Germany) equilibrated with buffer A at room temperature, followed by an extensive rinse with buffer B and a stepwise elution using buffer C. Purified L7ae was concentrated to greater than 500μM using a 5kDa Amicon

spin concentrator (Millipore, Billerica, MA, USA) and subsequently dialyzed and stored in buffer A at 4°C.

2.3.2 Over expression and purification of aFib

The aFib gene was cloned into pET3d^{Amp} expression vector (no purification tags) using the NcoI and BamHI restriction sites, and transformed into BL21 (DE3) cells already containing the pLysS^{Cm} vector. Transformed cells were grown, expressed, and harvested as described above for L7ae. Cells that were shown to over express aFib were lysed and centrifuged as described above for L7ae in buffer D. The aFib was then purified from the lysate using thermoprecipitation for 4 minutes at 85°C, and subsequent application to a 24mL Superdex200 size exclusion chromatography (SEC) column (Amersham Biosciences; Pittsburgh, PA, USA) equilibrated at 4°C in buffer D. The purified aFib was then concentrated to greater than 200μM using a 10kDa Amicon spin concentrator and dialyzed into buffer A for storage at 4°C.

2.3.3 Over expression and purification of aFib_n56

The truncated aFib_n56 mutant was also cloned into pET28a^{Kan} vector using the NheI restriction site and subsequently transformed into BL21 (DE3) cells. The cell growth, expression, and purification of 6x His tagged aFib_n56 was performed as described above for L7ae, with the following changes. Cells were lysed in buffer F (10mM Tris (pH8.0), 100mM NaCl, 20% (v/v) Glycerol, 4.0M Urea) and then applied to the Ni-NTA column also equilibrated in buffer F. The column was rinsed using buffer G (buffer F with 25mM Imidazole) and eluted using buffer H (buffer F with 400mM Imidazole). The protein was then loaded onto the SEC column equilibrated with buffer A (10mM Tris (pH8.0), 100mM NaCl, 1mM BME) as described above for aFib. Following

SEC, the protein samples were incubated with thrombin to cleave the 6x His tag. This step resulted in the removal of 17 amino terminal amino acids, leaving a total of 6 extra amino acids at the amino terminus. Cleaved aFib_n56 was separated from the uncleaved protein by batch binding to Ni-NTA agarose at room temperature in buffer B followed by elution with buffer C. The cleaved protein (unbound) was concentrated to greater than 200μM using an Amicon spin concentrator (10kDa) and dialyzed into buffer A for storage at 4°C.

2.3.3 Over expression and denatured purification of Nop5

The Nop5 gene sequence was cloned into pET28a^{Kan} using the NheI restriction site and transformed into BL21 (DE3) cells. Cells were grown in LB media as described previously, however after induction the cells were incubated at 22°C overnight for over expression. Cells were pelleted and lysed in buffer I (50mM Tris (pH 8.0), 400mM NaCl, 8.0M Urea) and subsequently centrifuged as described for the previous proteins. The lysate was then applied to a Ni-NTA agarose column equilibrated with buffer I, rinsed with buffer J (buffer I plus 25mM Imidazole) and subsequently eluted with buffer K (buffer I plus 400mM Imidazole). After elution from the Ni-NTA agarose column, the sample was dialyzed back into buffer I and injected onto a Superdex200 SEC column equilibrated with buffer I at 4°C. SEC fractions containing Nop5 were pooled and concentrated using an Amicon 5kDa spin concentrator to greater than 200μM and stored at 4°C.

2.3.4 Purification of T7-RNA polymerase

BL21 (DE3) cells transformed with the T7 polymerase gene and over expressed as described above for L7ae. Harvested cells were lysed and applied to a Ni-NTA column in buffer L, followed by a rinse with buffer M and elution with buffer N. The collected eluent was applied to a Superdex200 column equilibrated with buffer O. SEC fractions containing T7 polymerase were pooled and batch incubated with Affi-gel blue resin to remove any RNase contamination. 2μL of the resulting supernatant was incubated with 0.5μL of 0.8μg/μL MS2 RNA for 36h and subsequently visualized on a 15% urea polyacrylamide gel to confirm samples were RNase free. RNase free samples were concentrated to 75μM and dialyzed into buffer P prior storage at -20^{o}C.

2.3.5 *In vitro* transcription of RNA

The DNA sequences encoding for sR1 and sR8 (Table 2) were purchased from BioBasic in the pUC57^{Amp} vector and the template sequence was amplified by polymerase chain reaction (PCR). PCR transcription templates were analyzed for RNase contamination by 24h incubation with MS2 RNA and visualization on a 15% urea polyacrylamide gel. *In vitro* transcription reactions were prepared with the templates according to table 3 below, and allowed to run overnight at 37°C.

Table 2.2. DNA template sequences for the *in vitro* production of sRNAs.

sRNA	PCR Amplified DNA Template Sequence
sR1 (83nt)	cgccaa gctttaatac gactcactat agcagatgat gaattcccga tagtacgatt gatgagctaa actcccatgg actgatt
sR8 (81nt)	cgccaa gctttaatac gactcactat aggaaatgat gagggttcca gagctgaagc gtgatgaatg gttgacacgc tgacc

Table 2.3. Recipe for *in vitro* transcription reaction.

Component	Volume (μL)	Final Concentration
Deionized H_2O	327	
5x Buffer	200	1x
100mM DTT	100	10mM
25mM NTPs	120	3mM
100mM GMP	50	5mM
0.5U/μL iPPase	20	0.01 U/μL
T7-RNA Polymerase	80	0.3μM
40 U/μL RNase Inhibitor	3	1 U/μL
Template DNA	100	10% (v/v)

Following overnight transcription (greater than 12hours), the reactions were incubated an additional hour in the presence of DNase to hydrolyze the template DNA. Reactions were stopped by the addition of 100μL of 20% (w/v) potassium acetate (pH 5.2) and a phenol extraction was performed on the sample to extract all protein components. The remaining nucleic acids were precipitated with 95% ethanol at -20°C for 48 hours, followed by a 15 minute centrifuge at 13,000 rpm (4°C). Nucleic acids were washed with room temperature 75% ethanol, centrifuged at 13,000 rpm (22°C) and resuspended in 500μL RNase-free water. Another 100μL of 20% (w/v) potassium acetate (pH 5.2) was added to the sample and the nucleic acids were precipitated a second time as described above. The quantity and purity of the final RNA samples were assessed by measuring the absorbances at 260 and 280nm.

2.4 Ni-NTA based pulldown assay

1.0nmole of His-tagged Nop5 (40μL of 25μM) was applied to 50μL of Ni-NTA slurry equilibrated in buffer I using batch methods. The Ni-NTA resin was then rinsed and equilibrated into buffer Q as a preparation for the binding of aFib. 4.0nmole of

Fibrillarin (40µL of 100µM in buffer Q) was applied to the resin and allowed to interact with Nop5 bound to the resin. Following incubation, the resin was transferred to a 0.22µm spin filter (Millipore) and centrifuged at 400x*g* for 10 minutes to remove all excess Fibrillarin and buffer from the resin. The resin was then transferred to a fresh 0.22µm spin filter and eluted with 40µL buffer R and centrifuged at 400x*g* for 10 minutes. Protein samples were visualized on a 15% SDS-PAGE gel and quantified using ImageJ software (Abramoff *et al.* 2004).

2.5 Electrophoretic Mobility Shift Assay (EMSA)

sR1 RNA (250pmoles) was mixed with varying amounts of L7ae (100-1200pmoles) in a total volume of 7µL buffer S. Samples were incubated at room temperature for 15 minutes before being loaded onto a 15% Native RNA PAGE Gel. Gel mobility of the RNA samples was visualized with a UV transilluminator after ethidium bromide staining and band intensities were measured using ImageJ.

2.6 Measuring binding of L7ae to sR1 RNA by Isothermal Titration Calorimetry

Prior to ITC experiments, solutions were centrifuged at >10000x*g* in an Eppendorf 5414C microcentrifuge (Eppendorf; Westbury, NY, USA) for 10 minutes at 20°C. Solutions were then degassed and thermoequilibrated in a ThermoVac device (MicroCal™; Northampton, MA, USA) for 5 minutes. Approximately 1.4mL of the degassed RNA was loaded into the sample cell of a VP-ITC MicroCalorimeter (MicroCal™) and subsequently thermoequilibrated. Approximately 300µL of degassed L7ae protein was then loaded into the injection syringe and underwent a double purge-refill cycle to ensure a complete bubble free filling. The injection syringe was then inserted into the sample cell and a reference power baseline was established at 0.055J/s

during which the injection syringe was stirring at 160rpm. Upon complete baseline equilibration, the isothermal titration experiment was started. Following each baseline equilibration, 5-15μL of L7ae was titrated into the sample cell over a period of 10-25 seconds. Thermostabilization was monitored throughout each titration experiment consisting of a total of 20-25 consecutive injections. The thermostability data was plotted and analyzed using the MicroCal™ Origin7 software and peaks corresponding to the power required to return the sample cell to the same temperature as the reference cell were integrated and plotted as a function of the L7ae concentration. Binding constants were obtained through curve fitting the resulting data with a single set of sites model (Fersht 1999). Additionally, L7ae-RNA samples were extracted from the sample cell and analyzed on a 15% Urea/Acrylamide gel.

CHAPTER 3: ASSOCIATION OF FIBRILLARIN WITH NOP5

Unlike previously characterized Fibrillarins, the *S. acidocaldarius* enzyme has been shown to form homodimers in solution (Burke 2006). This presents the possibility for an additional intermediate complex to be formed through a Fibrillarin homodimer bound to a single Nop5, rather than the singly bound Fibrillarin state previously observed. The first step to investigating the possible assembly of this intermediate complex is the purification and storage of the two protein subunits.

3.1 Purification of Archaeal Fibrillarins.

The purification of aFib was successful using thermoprecipitation (Ziesche *et al.* 2004) followed by SEC fractionation. The fractions collected from the SEC were concentrated and run on a 12% SDS-PAGE gel for visualization as shown in Figure 3.1a below. Alternatively, the recombinant 6x His tagged aFib_n56 was successfully purified using Ni-NTA agarose. This protein was eluted, concentrated and analyzed by 12% SDS-PAGE gel as well (Figure 3.1b). In both cases, the Fibrillarin samples migrate as both a monomer and an SDS stable dimer, however, it should be noted that aFib_n56 dimers are always seen to have a larger apparent molecular weight than the wild type aFib.

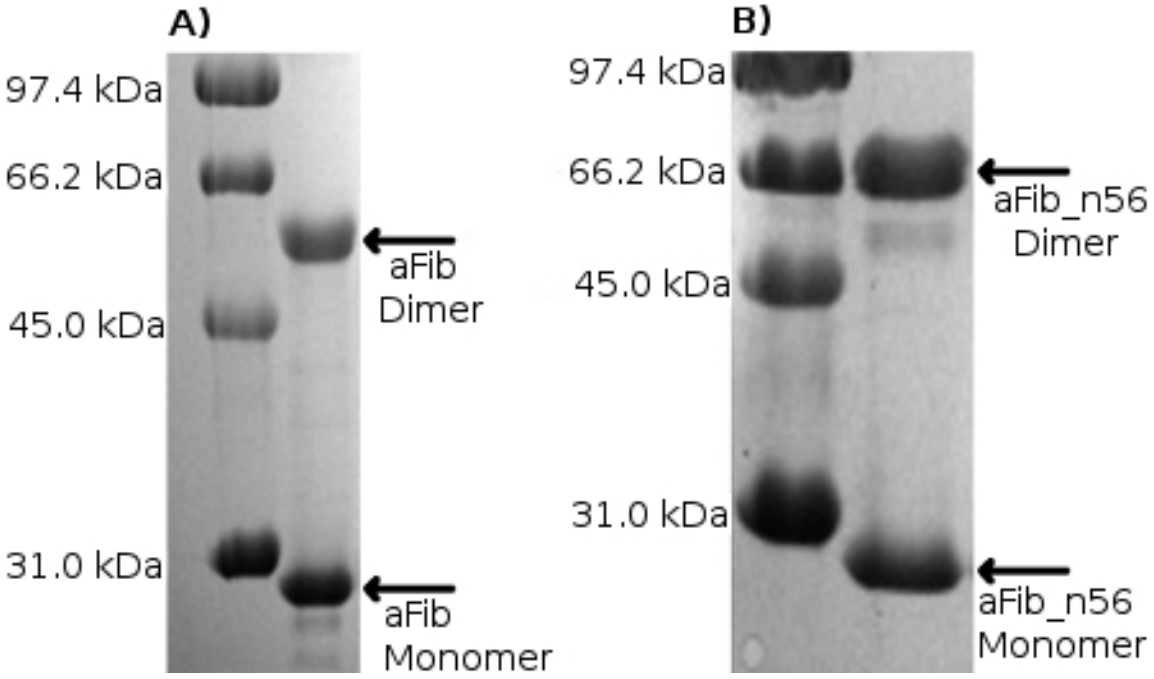

Figure 3.1. 12% SDS-PAGE gels illustrating A) purified aFib B) a purified aFib_n56. Both samples show the formation of SDS stable dimers and aFib_n56 dimers are seen to migrate slower than aFib (having a higher apparent molecular weight).

3.2 Purification of Recombinant 6x His Tagged Nop5

3.2.1 Purification by immobilized metal affinity chromatography

Initial purifications of Nop5 were performed using nickel immobilized metal affinity chromatography (IMAC). Following elution from the resin, the samples were visualized by coomassie brilliant blue (R250) stained SDS-PAGE. These gels (Figure 3.2) showed Nop5 to be contaminated with many lower molecular weight polypeptides. Given the sizes (smaller than Nop5) and similar binding affinities of the many contaminants, they may in fact be degradation products that arise during the overexpression and purification of Nop5. Cell lysis and purification of Nop5 in the presence of either PMSF or a complete protease inhibitor pellet does not improve purity, suggesting that post-lysis proteolytic degradation is not the primary source of the contaminants (Figure 3.3).

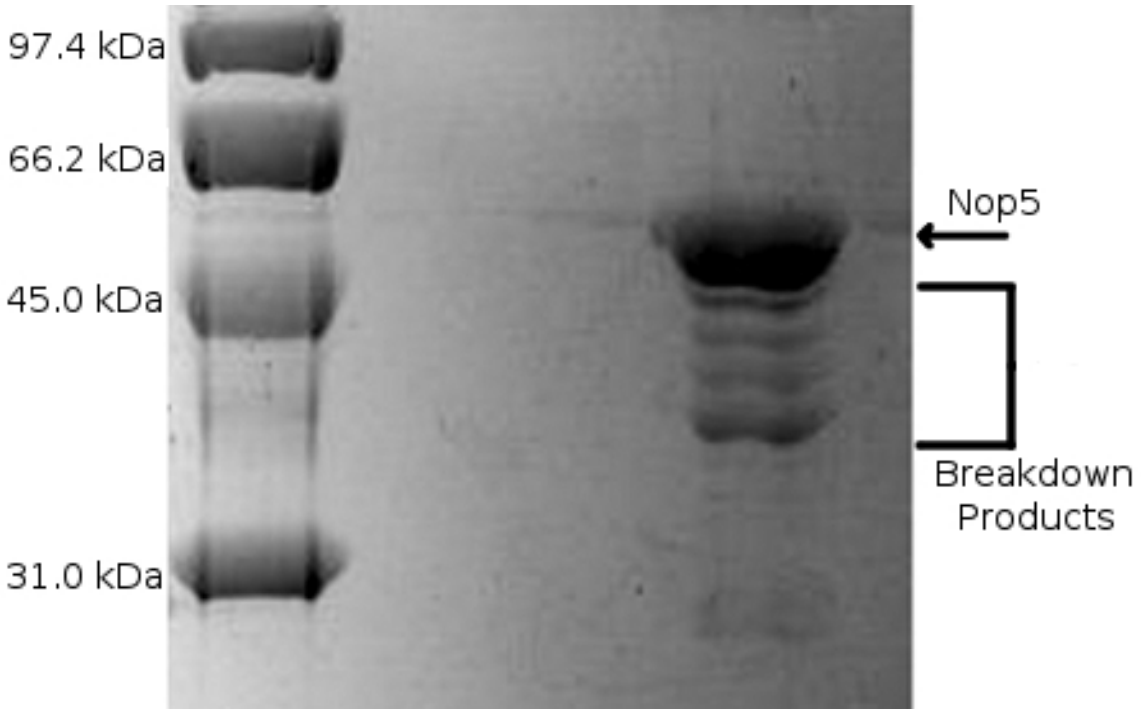

Figure 3.2. A 12% SDS-PAGE gel illustrating the impurities in Nop5 following elution from the IMAC column. As can be seen, there are many contaminants in the elution, and all appear to be of lower apparent molecular weight than full length Nop5.

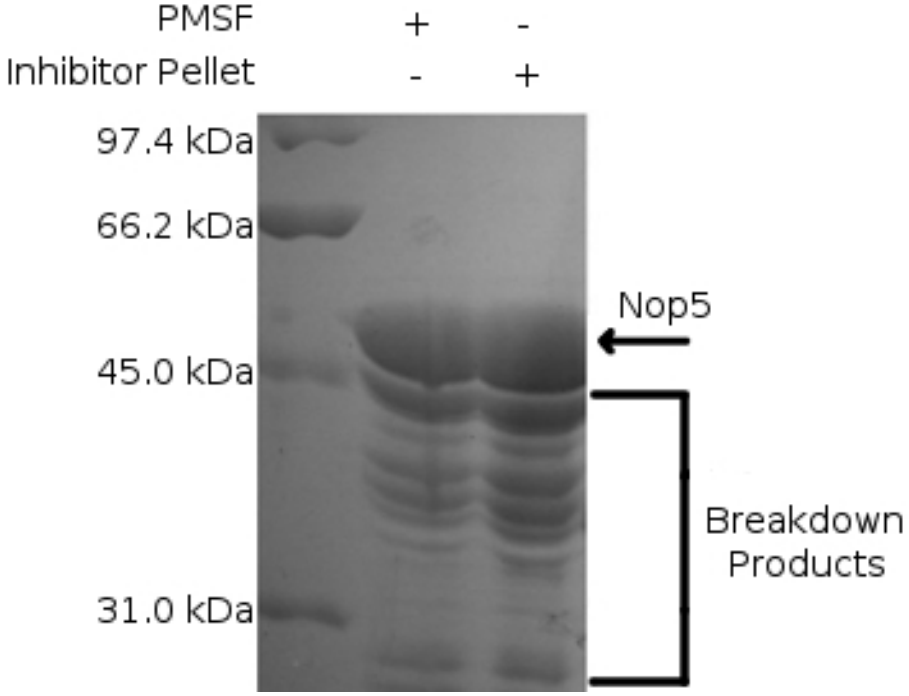

Figure 3.3. A 12% SDS-PAGE gel that illustrates that PMSF (lane 2) and a complete protease inhibitor (lane 3) have no apparent effect on the contaminating peptides present after Ni-NTA purification of Nop5.

3.2.2 Double transformation with aFib and Nop5

In vivo, Nop5 exists as a heterodimer with Fibrillarin (Tran et al. 2003). Our initial attempts to purify recombinant Nop5 (Section 3.2.1) suggest that it may undergo context dependent folding and may be subject to cellular degradation pathways in the absence of Fibrillarin. In order to test this hypothesis, a pET3d^{Amp} plasmid containing the aFib gene was transformed into BL-21 DE3 cells already containing the plasmid with the Nop5 gene (pET28a^{Kan}). Transformations were plated on LB-agar containing both ampicillin and kanamycin, successfully selecting for only the clones which contained both plasmids. Transformants were tested for the co-expression of Nop5 and aFib by induction with IPTG. As seen in Figure 3.4 below, both proteins were over expressed by transformant 2 (lanes 4/5).

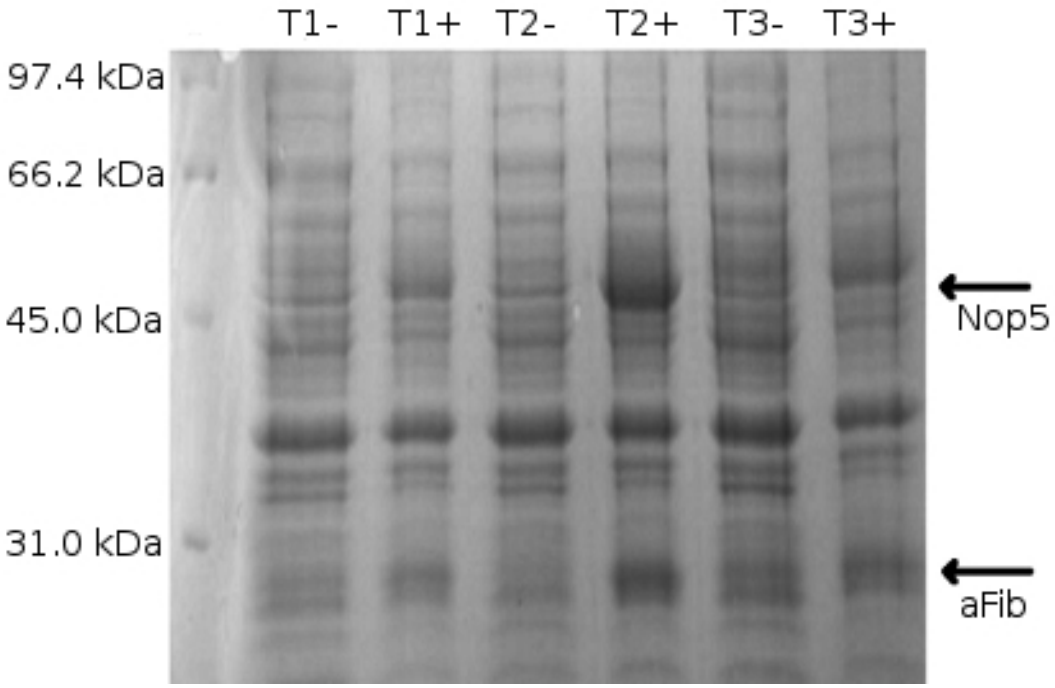

Figure 3.4. An over expression test of BL-21 DE3 cells co-transformed with Nop5 and aFib. Lane 1 is a low molecular weight marker and the subsequent lanes are alternating -/+ for IPTG. Transformant 2 (lanes 4/5) shows the expression of both Nop5 (48.9kDa) and aFib (26.4kDa).

The aFib and Nop5 double transformants were over expressed and lysed as previously described and purified by IMAC. Purified samples were then analyzed by SDS-PAGE, shown in Figure 3.5 below. Nop5 (His-tagged) and aFib (no tag) co-purify, suggesting a Nop5/aFib heterodimer is formed *in vivo*. Further, contaminating bands that are present when Nop5 is over expressed and purified alone are virtually eliminated. To separate the Nop5 from the aFib, the heterodimer was bound to the resin and rinsed with buffer I (50mM Tris (pH 8.0), 400mM NaCl, 8M urea) to elute the aFib subunit. Following aFib separation, the Nop5 was renatured by rinsing with 50mM Tris (pH 8.0), 400mM NaCl and eluted using the same buffer plus 400mM imidizole. Purification of Nop5 by this method appears to be successful, however the Nop5 samples were unusable in binding assays because they precipitated shortly after elution.

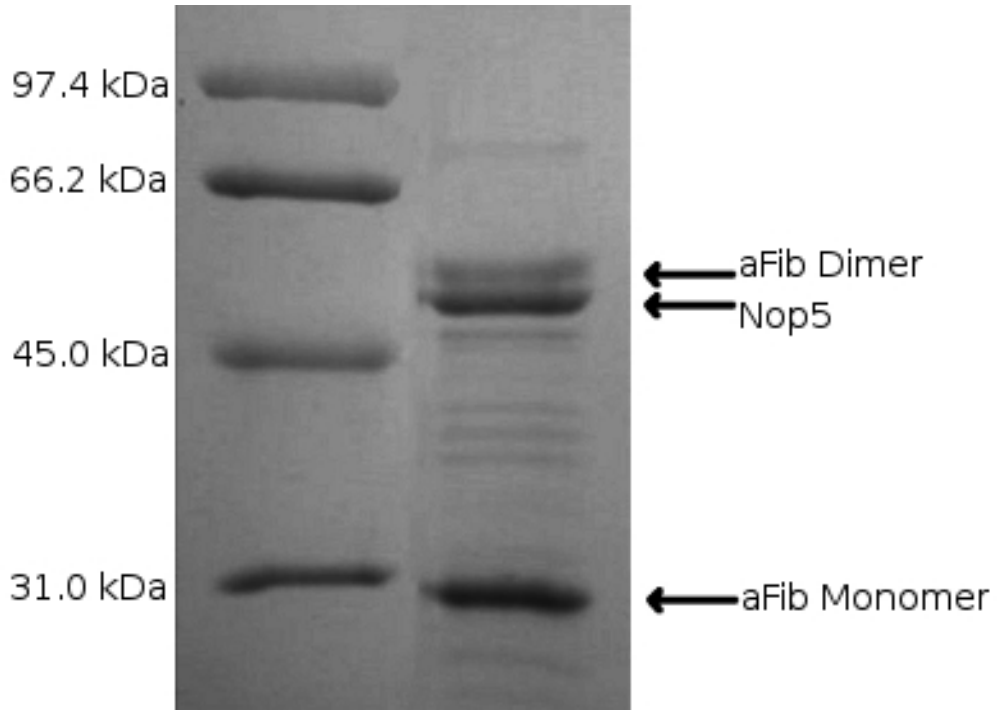

Figure 3.5. A 15% SDS-PAGE gel showing the Ni-NTA agarose co-purification of Nop5 and aFib. Both proteins are present in the eluent and there are fewer contaminating peptides present than observed when Nop5 is over expressed and purified alone. Unfortunately, once aFib was removed Nop5 again readily precipitated.

Improved purification through co-transformation supports the suggestion that Nop5 may be improperly folded on its own and requires stabilization. Since temperature is also known to affect protein folding, a lower expression temperature was also examined as a viable approach to improve purity. Figure 3.6 below shows the Nop5 elution from IMAC resin after an over expression at room temperature (22^{o}C). As seen with the co-expression technique, this approach also reduces the contaminating bands. Nop5 which was purified using this method also readily precipitates, again presenting difficulties for storage and use.

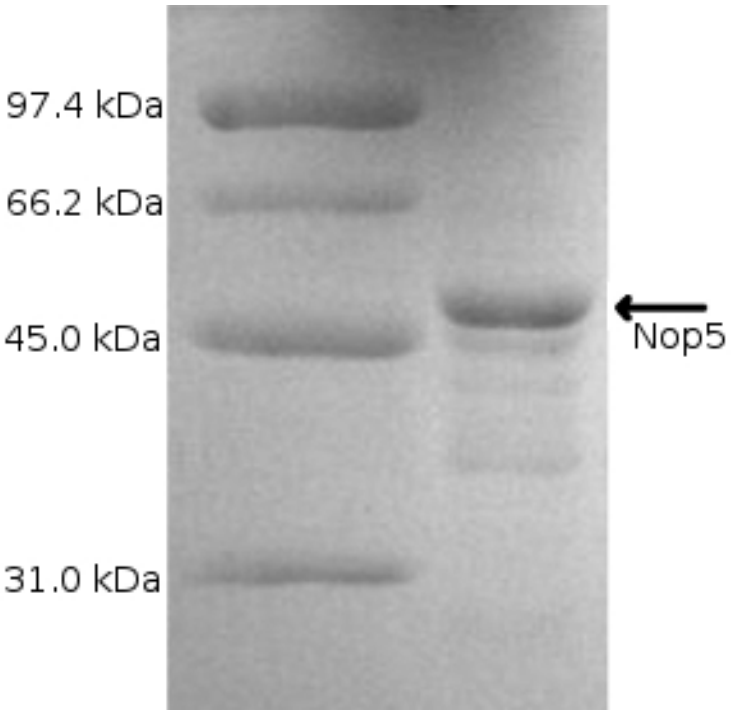

Figure 3.6. A 12% SDS-PAGE gel showing the IMAC purification of Nop5 following an overexpression at room temperature. As seen with the co-expression approach, the contaminating bands are nearly eliminated. Again, the samples precipitated shortly after purification.

The low solubility of Nop5 (maximum solubility is approximately 5μM) and the resulting high volumes of sample, made further purification by SEC under native conditions difficult. The solubility of Nop5 was assessed in a variety of buffers including

pH 5-9, different salts at concentrations up to 1M, 0-40% glycerol, and 0-8M urea. Unfortunately, of all the buffers, Nop5 is only soluble in the presence of the denaturant urea (8M).

3.2.3 Denatured (Urea) Purification of Nop5

Using a lower expression temperature (room temperature) combined with denaturing conditions (8M urea) during lysis and all subsequent stages of purification may generate stable Nop5 that could be further purified and stored long term. Using this approach, denatured Nop5 was eluted from the Ni-NTA agarose beads and consistently concentrated to greater than 200μM. These samples were then applied to the SEC for further purification. The SDS-PAGE gel in Figure 3.7 below, illustrates typical fractions collected from the SEC200 column under denaturing conditions (A) and the final purified Nop5 stored for later use (B). When comparing this purification with those previously described above, this method shows fewer and less prevalent contaminating bands and was, therefore, selected for all subsequent Nop5 purifications.

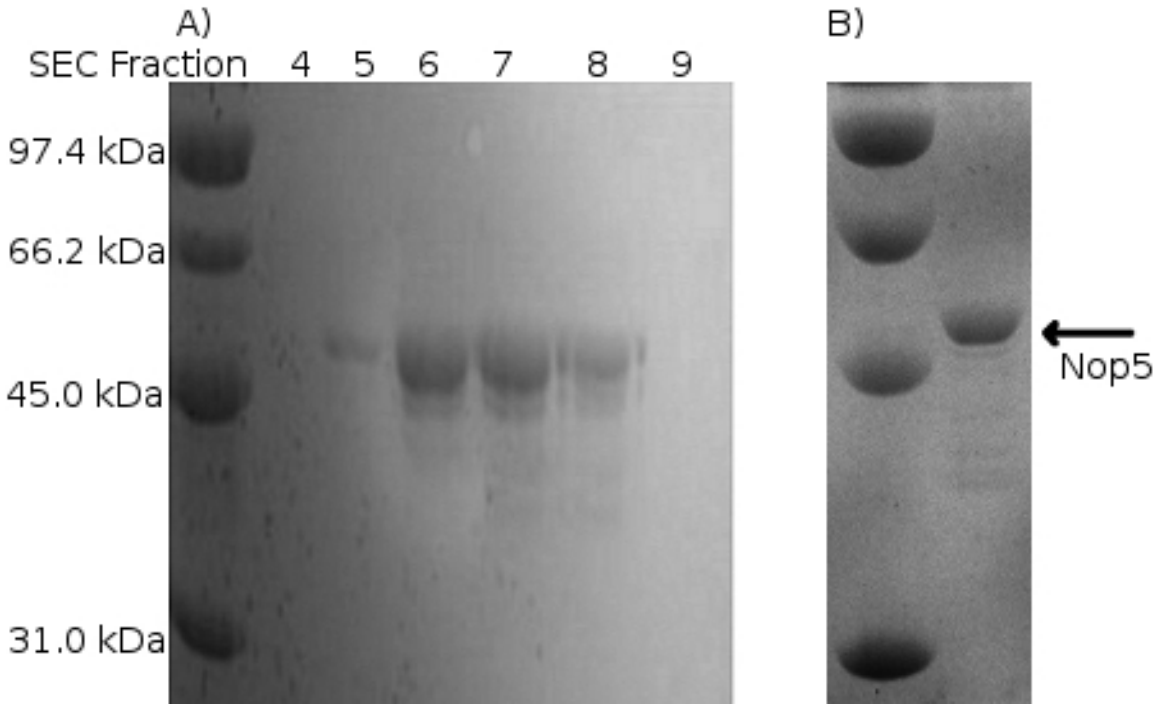

Figure 3.7. A 15% SDS-PAGE gel showing A) the fractions collected from an SEC200 column under denaturing (8M urea) conditions and B) pooled and concentrated Nop5 prepared for storage. Nop5 is clearly present and the contaminating polypeptides appear to be fewer and less prevalent than the previous approaches described above.

3.3 Ni-NTA agarose based pulldown assay

Since the Nop5 is solubilized by 8M urea, any data obtained from ITC experiments would contain a signal for both the binding interaction (Fibrillarin binding to Nop5) and the renaturing of Nop5 after the urea becomes diluted. Because of this, ITC cannot be used to analyze the binding interactions between Nop5 and Fibrillarin and an alternative approach was required. One alternative approach to investigate the Nop5-Fibrillarin interaction is to utilize Ni-NTA as a scaffold to sequentially assemble an sRNP intermediate complex. In this approach, only one of the subunits can be allowed to interact with the resin. We chose to immobilize Nop5 on the resin and utilized this assembly to pull out aFib. If aFib cannot interact with the resin, any present during elution must be bound to Nop5 and the stoichiometry of this interaction can be

determined. Using this approach, we examined whether dimeric Fibrillarin was able to interact with monomeric Nop5.

3.3.1 Controls

It was hypothesized that an sRNP intermediate Fibrillarin could be fished out of solution using Nop5 as a scaffold. Because the purified Nop5 protein contains a 6x His tag, it could be immobilized on nickel IMAC beads. By incubating Nop5 with Ni-NTA resin under denaturing conditions (8M urea), the coiled-coil domain is denatured and Nop5 is likely to bind as a monomer. The aFib samples could then be exposed to the resin and allowed to interact with the pre-bound monomeric Nop5. Any intermediate complexes could then be eluted.

In order to utilize Nop5 as the fish hook it needs to have a strong binding interaction with the resin. It must also be completely recovered during the elution stage to allow for a stoichiometric analysis. Figure 3.8 below demonstrates that Nop5 can be successfully bound to the resin in buffer I (50mM Tris (pH 8.0), 400mM NaCl, 8.0M urea), renatured and equilibrated into the aFib binding buffer Q (10mM Tris (pH 8.0), 100mM NaCl, 1mM BME, 25mM Imidazole), and eluted with high recovery using buffer R (buffer Q with 400mM imidazole and 0.1M EDTA). Notably, Nop5 does not appear to be lost during the rinse and equilibration steps.

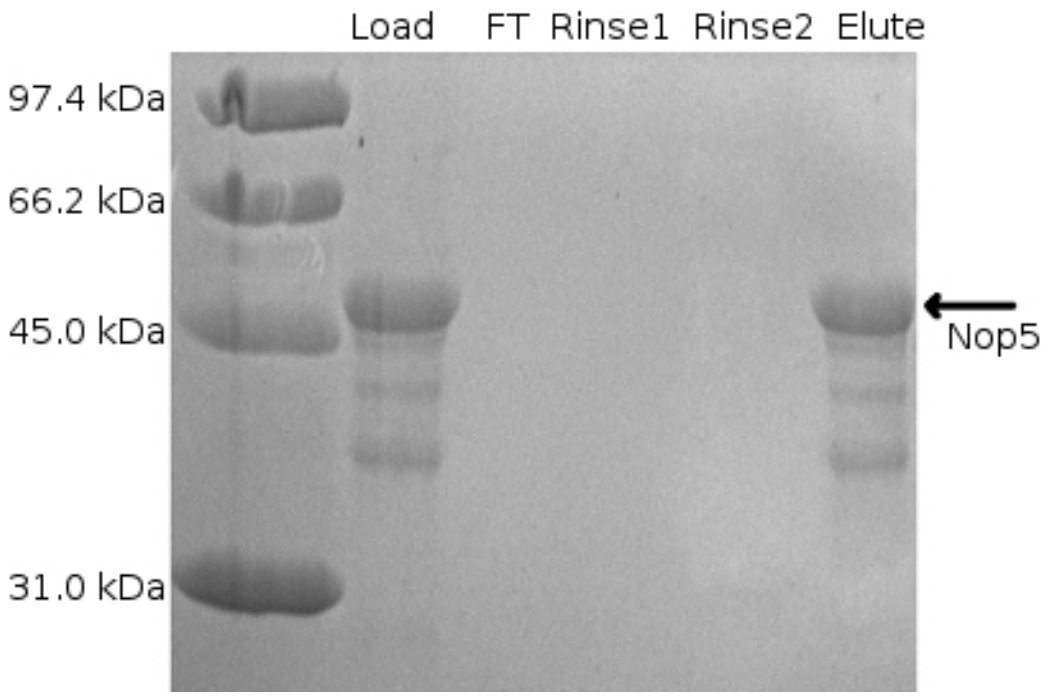

Figure 3.8. A 15% SDS-PAGE gel demonstrating Nop5 quantitatively binds and elutes from the resin.

Wild type Fibrillarin (aFib) is not tagged and should not be capable of interacting with the Ni-NTA resin. Figure 3.9 below illustrates that when aFib is applied to the resin in buffer Q (lane 2), most of the aFib is recovered in the flowthrough (lane 3). The first rinse step (lane 4) still contains some excess unbound aFib but the second rinse (lane 5) and elution (lane 6) have no detectable aFib content. This suggests that aFib does not interact with the Ni-NTA agarose.

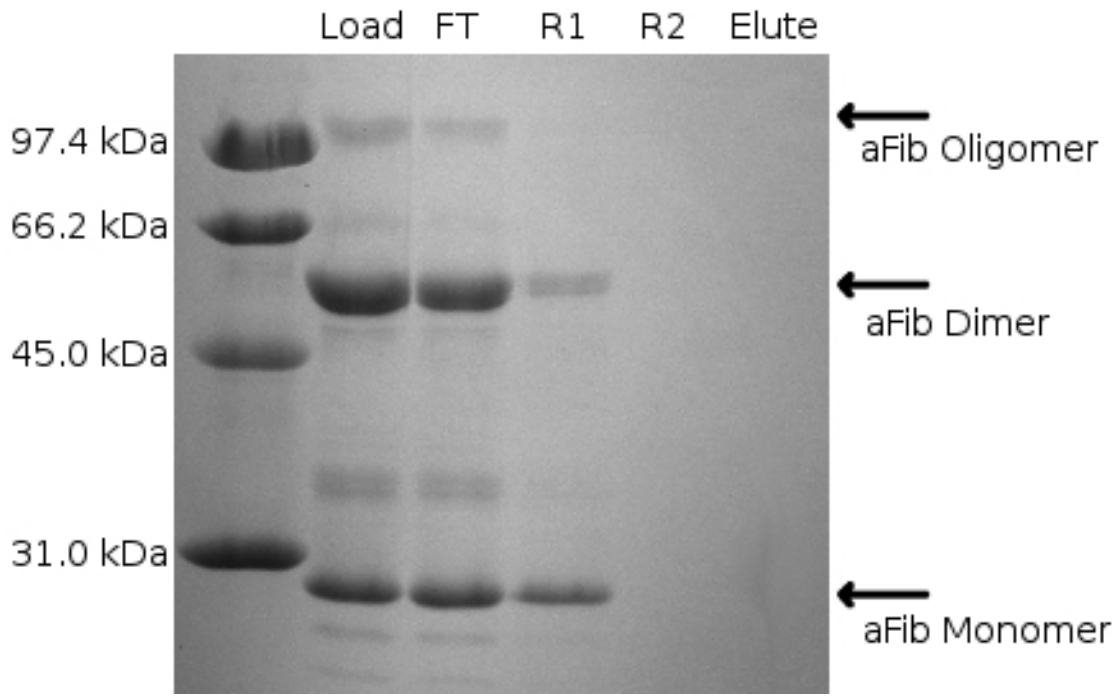

Figure 3.9. A 15% SDS-PAGE gel illustrating that aFib does not bind to the Ni-NTA agarose in buffer Q. aFib that is applied to the resin (Load) is found in either the flowthrough (FT) or the first rinse (R1). Rinse 2 and elution do not contain any detectable aFib.

Unlike aFib, aFib_n56 contains a 6x His tag and was purified through affinity chromatography (Ni-NTA agarose). Removing the 6x His tag from aFib_n56 through thrombin cleavage was successful, as demonstrated by the reduced apparent molecular weight seen in lane 3 of Figure 3.10. Further testing confirms that the aFib_n56 is cleaved and no longer able to interact with the Ni-NTA agarose (Figure 3.11). Again, the protein is mostly present in the flowthrough (lane 3), with the remainder being recovered during the first wash (lane 4). This result is consistent with what was seen previously for aFib.

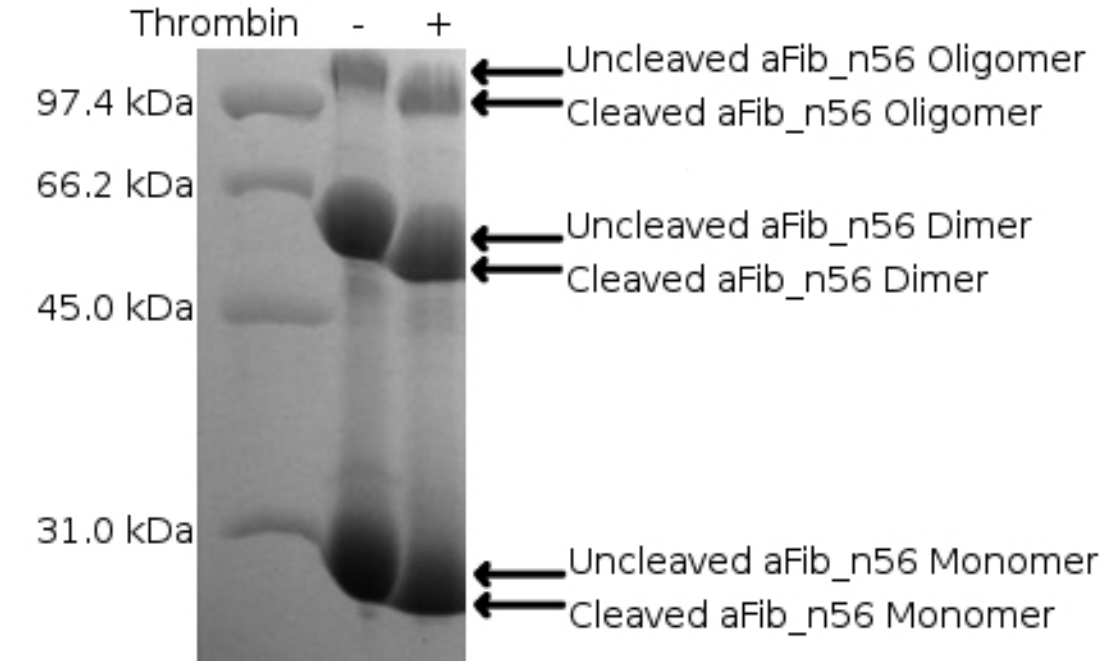

Figure 3.10. A 15% SDS-PAGE gel illustrates the successful cleavage of aFib_n56. There is a decrease in apparent molecular weight between the untreated (lane 2) and thrombin treated (lane 3) aFib_n56. The decrease in apparent molecular weight of the protein suggests thrombin cleavage is successful.

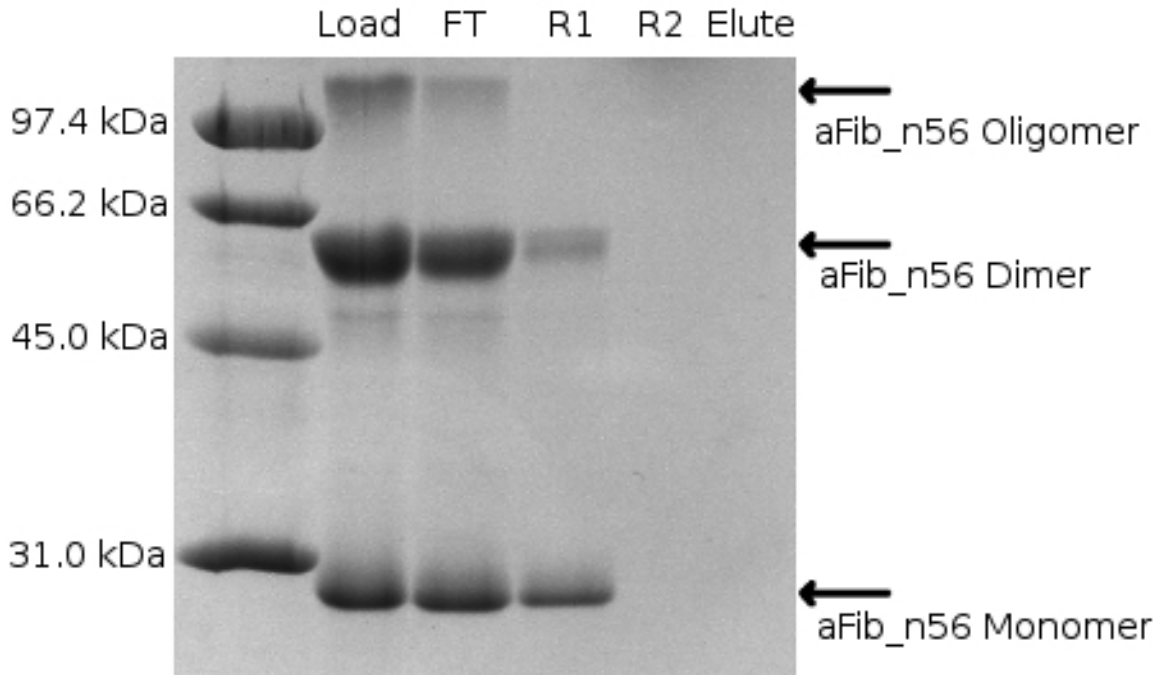

Figure 3.11. A 15% SDS-PAGE gel illustrating that cleaved aFib_n56 cannot interact with the Ni-NTA agarose in buffer Q. Thrombin cleaved aFib_n56 that is applied to the resin (Load) is recovered in either the flowthrough (FT) or the first rinse (R1). Rinse 2 and elution do not contain any detectable aFib_n56.

3.3.2 Progress towards a Ni-NTA agarose based pullout assay to assemble an archaeal sRNP intermediate.

Initial assays demonstrated that aFib does in fact interact with Nop5 immobilized on the resin (shown in Figure 3.12). In this experiment, aFib (lane2) was incubated (in the absence of denaturant) with Nop5 prebound to Ni-NTA agarose. Following incubation, the excess aFib was rinsed away (lane 4) and the remaining complexes were eluted (lane 5). In this experiment, Fibrillarin can facilitate the correct folding of Nop5 to allow the aFib-Nop5 heterodimer interaction form (context dependent folding). Densitometric analysis of the elution yields a ratio of 1.03 aFib per Nop5. The rinse stage is important because the Ni-NTA resin is suspended in a small amount of buffer (even after decanting the supernatant) and some of the unbound aFib will remain in this solution. Rinsing the resin with buffer will rapidly remove this additional aFib (as we did above), however this could potentially also break weak non-covalent interactions, such as those responsible for the aFib dimer.

.

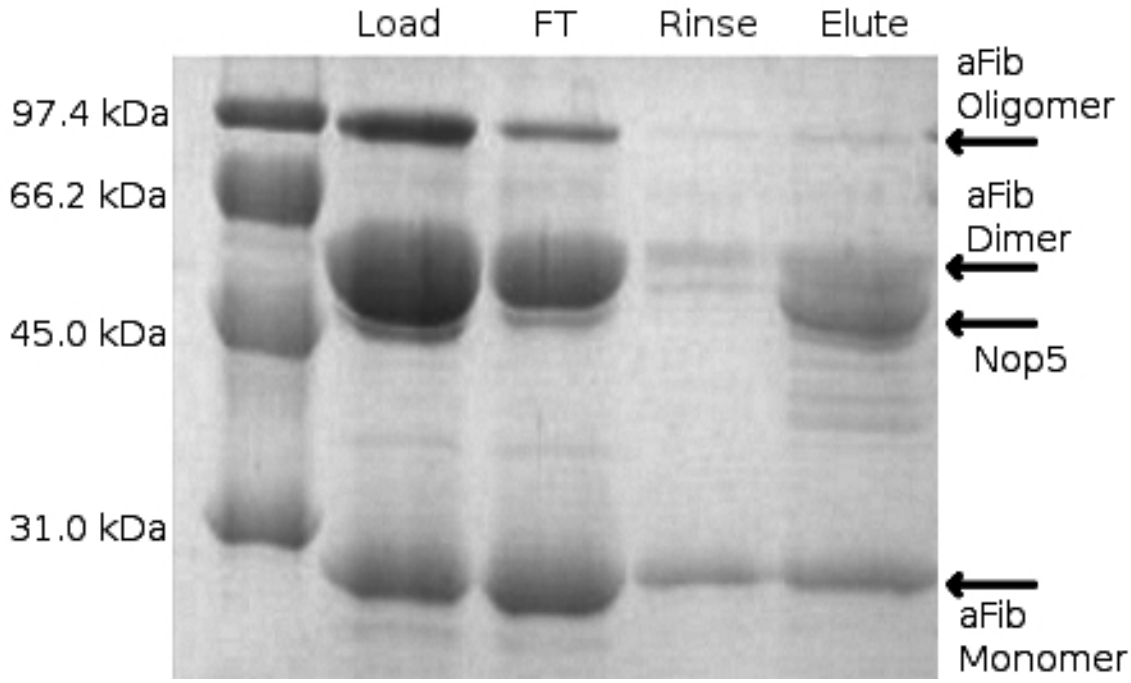

Figure 3.12. A 15% SDS-PAGE gel demonstrating that aFib applied to the immobilized Nop5 (Load) is able to form an intermediate complex in the absence of L7ae and sRNA. Lane 3 (FT) shows the excess aFib removed in the supernatant, and lane 4 (Rinse) also appears to contain aFib. Eluting the intermediate complex yields approximately one aFib bound to each Nop5 molecule.

To investigate any potential rinsing effects on the formation of an aFib dimer, subsequent pullout assays utilized a 2μm spin filter rather than rinsing. The excess buffer/protein is completely removed by trapping the Ni-NTA agarose on a filter prior to elution and centrifuging the buffer away. Figure 3.13 below represents a typical 15% SDS-PAGE visualization of the pullout assay performed with the spin filter approach. As can be seen, both Fibrillarin constructs are fished out and can be co-elute with Nop5 at much higher levels than the previous approach. This revised pullout assay yielded densitometric ratios of 1.94 aFib (lane 10) and 1.97 aFib_n56 (lane 11) bound to each copy of Nop5. This suggests that the rinse stage is in fact having an effect on the aFib dimer and should be avoided.

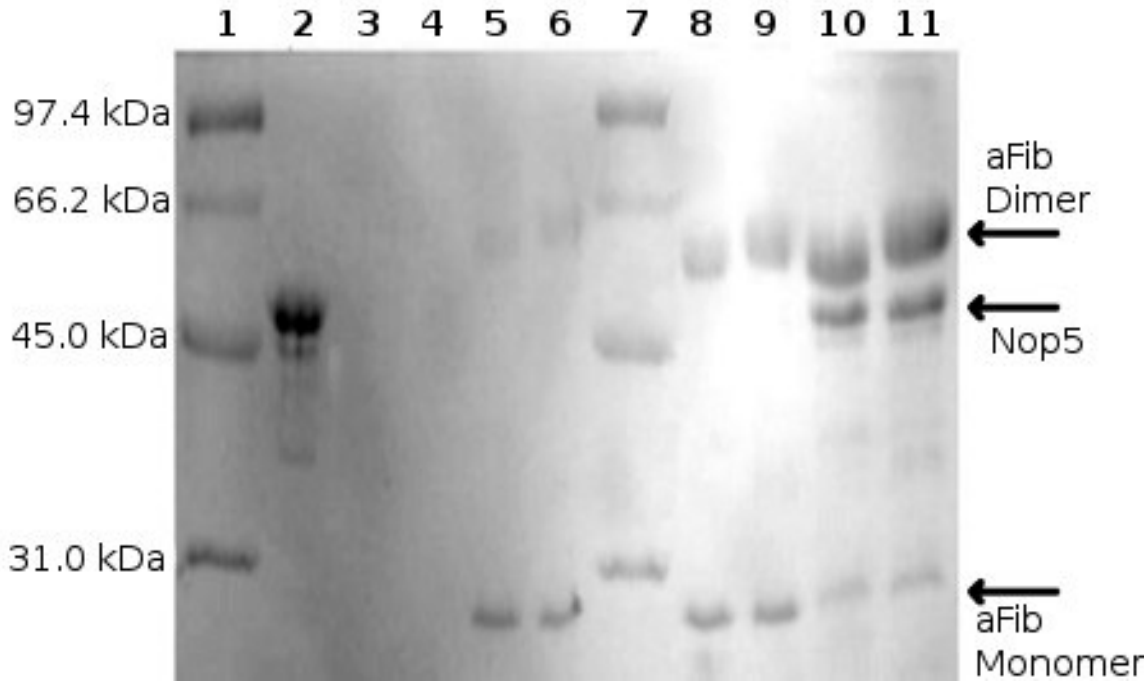

Figure 3.13. A Nop5-aFib pullout assay visualized on a 15% SDS-PAGE gel. Nop5 is bound to the resin (lane 2) and is equilibrated into the aFib buffer without losses (lane 3/4). aFib (lane 8) and thrombin cleaved aFib_n56 (lane 9) is then incubated with the resin. Excess aFib and aFib_n56 is then removed by centrifugation through a 2μm spin filter (lane 5/6). Elution using this approach yields a ratio of 1.94 (Wt) and 1.95 (n56) Fibrillarin co-eluting with Nop5.

3.4 Discussion

The *in vitro* methylation assays (Tran *et al.* 2003) and cooperativity studies (Bortolin *et al.* 2003; Omer *et al.* 2006) show that a symmetric complex containing two copies of the sRNP (Fibrillarin, Nop5, L7ae) is required for efficient methylation of substrate RNA. The X-ray crystal structures of the Nop5-Fibrillarin intermediate complex presented by Aittaleb *et al.* (2003) and Oruganti *et al.* (2007) both show the presence of two Fibrillarin molecules, one bound to each of the Nop5. However, in the absence of Nop5, the Fibrillarin structure obtained by Wang *et al.* (2000) contains two Fibrillarin molecules forming a homodimer.

Since Nop5 can be immobilized on Ni-NTA agarose under denaturing conditions (purified in 8M urea), we chose to use this as a "fish hook" to catch aFib in a pullout assay. This approach involves immobilizing Nop5 on the resin (denatured), followed by buffer exchanges to remove the denaturant. When either aFib or aFib_n56 is applied to the pre-bound Nop5, followed by rinsing to remove excess protein, Fibrillarin can be detected in the eluent along with Nop5. If equivalent amounts of lysozyme or bovine serum albumin are applied to the immobilized Nop5, neither can be detected in the eluents. This suggests that Fibrillarin forms a specific interaction and demonstrates that this new pullout method is a useful tool to investigate the context dependent folding of Nop5.

Once we confirmed that the Fibrillarin Nop5 interaction could be detected with this approach, increased concentrations of aFib were applied to the Nop5 "fish hook" to determine if dimeric aFib could also be bound. We found that applying dimerizing concentrations of Fibrillarin to the Nop5 still resulted in a 1:1 molar ratios being eluted (Figure 3.12). The current approach to remove any excess unbound aFib from resin was to rinse the samples prior to elution. The relatively high K_d for aFib dimerization (61.9μM) suggests that the rinse step could actually be breaking this interaction, resulting in a single, monomeric aFib bound to Nop5 (as we detect). Subsequent experimentation and optimization verified that the Ni-NTA agarose beads (with the proteins bound to them) could be filtered by centrifugation through a 0.2μM membrane without breaking the protein interactions (aFib and Nop5 could still be recovered in a 1:1 ratio). Using this revised approach, we were able to detect molar ratios approaching two aFib molecules per Nop5 bound. This suggests that the formation of a Fibrillarin homodimer does not

prevent the formation of a heterodimer with Nop5, and that both interactions can occur simultaneously.

When high concentrations of aFib_n56 (previously shown unable to form the homodimer (Burke 2006)) are applied to the pre-bound Nop5 under non denaturing conditions, we still obtain a 2:1 stoichiometry. Since the Fibrillarin dimer cannot be formed, we tested for the possibility of non-specific binding by using a competition assay. A low concentration aFib_n56 was applied to pre-bound Nop5 and the excess protein was rinsed away. We then incubated this pre-formed Nop5-aFib_n56 complex with a low concentration of aFib, again rinsing away any excess protein after binding. The resulting complexes were then eluted and analyzed by SDS-PAGE, yielding a stoichiometry of 1.2 Fibrillarin per Nop5. A stoichiometry greater than 1:1 after multiple rinse cycles suggests that aFib_n56 does exhibit non-specific binding interactions.

Box C/D sRNPs are highly dynamic complexes (Omer *et al.* 2003). The current model for a complete Box C/D sRNP positions the two Fibrillarin active sites to far away to explain biological data. The domain rearrangements described by Oruganti *et al.* (2007) suggest a mechanism to swing the two Fibrillarins (each bound to a Nop5) close enough to solve the distance problem. Two new structures representing the complete box C/D sRNP (including substrate analogs) have recently emerged (Bleichert *et al.* 2009; Ye *et al.* 2009), which both illustrate domain arrangements conducive to the formation of the Fibrillarin dimer observed by Wang *et al.* (2000). Based on these structures and the work presented above, it is possible that upon binding substrate RNA the sRNP undergoes domain rearrangements to form the active conformation containing a Fibrillarin dimer.

This result would also explain why the Fibrillarin dimer was not identified in the earlier structures lacking substrate RNA.

In this chapter, we have shown that the modified pull down assay can be used to investigate the context dependent folding of Nop5 in the presence of Fibrillarin. Further, the Fibrillarin dimer observed by Wang *et al.* (2000) can also interact with Nop5, suggesting that both interactions can co-exist. While the role of a Fibrillarin homodimer is not yet fully understood, we suggest that it is likely required for sRNP catalysis and can only be detected when substrate RNA is present.

CHAPTER 4: A QUANTITATIVE ANALYSIS OF THE BINDING INTERACTIONS BETWEEN L7AE AND SR1 SRNA

While ITC experiments involving RNA have been successful in the past, working with RNA samples can be problematic (Buurma and Haq 2007). These experiments require a homogeneous RNA sample (both single species and conformationally homogeneous) and additional controls must also be run to confirm the integrity of RNA samples throughout the experiment (eg. RNA samples must be confirmed stable for the experiment duration and recoverable after completion). Further, all vessels, buffers and equipment to be used must be adequately cleaned and confirmed to be free of RNase contamination before use.

While the large sample sizes that are required for ITC experiments present a significant hardship, it is a powerful and versatile method to study the physical basis of molecular interactions (Salim and Feig 2009). Further, ITC can be used on native samples because it measures heat changes due to biological interactions and conformational changes, whereas alternative methods typically require the introduction of modifications or labels to generate a signal. ITC provides direct access to the enthalpy (ΔH), association constant (K_a) and stoichiometry (n) of the observed interactions and using K_a values from multiple temperatures to construct a Vant'Hoff plot yields thermodynamic parameters under standard conditions (enthalpy (ΔH^o), Gibbs free energy (ΔG^o) and entropy (ΔS^o)). The following work investigates the use of ITC to quantitatively study the interactions between L7ae and a representative sRNA, two components of the archaeal box C/D sRNP.

4.1 The expression and purification of recombinant 6x His tagged L7ae

In archaeal sRNPs, L7ae is the protein responsible for binding the k-turn of sRNAs. To probe the binding interactions between these two components, L7ae must be obtained in both high concentration and purity. L7ae purification was straight forward, purified by nickel affinity chromatography and subsequently concentrated to greater than 300μM (very high and sufficient for analyzing binding interactions). Analysis of the affinity chromatography eluent by SDS-PAGE (Figure 4.1 below) shows L7ae is the expected size (16.5kDa) and that greater than 99% purity has been achieved.

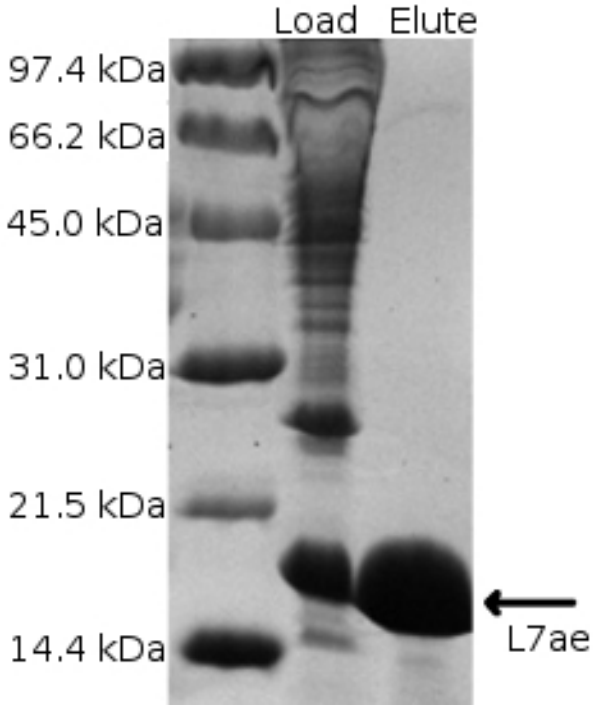

Figure 4.1. 15% SDS-PAGE gel showing the successful purification of L7ae by Ni-NTA agarose. L7ae runs at the expected size (16.5kDa) and shows greater than 99% purity.

4.2 The expression and purification of recombinant 6x His tagged T7-RNA Polymerase

A T7-RNA polymerase was produced in the laboratory to minimize the costs associated with the *in vitro* production of RNA. As seen in Figure 4.2 below, initial purification by nickel affinity chromatography was successful and further purity (greater than 99%) was obtained by applying the eluent to an SEC75 column (fractions shown in Figure 4.3A). Finally, the samples were incubated with Affi-gel blue gel to selectively remove RNase contaminants. The 12 hour RNase test analyzed by ethidium bromide stained Urea-RNA PAGE confirms that the purified T7-RNA polymerase is free of RNase contamination (Figure 4.3B below). T7-RNA polymerase was stored in buffer P at -20^{o}C until needed for transcription reactions.

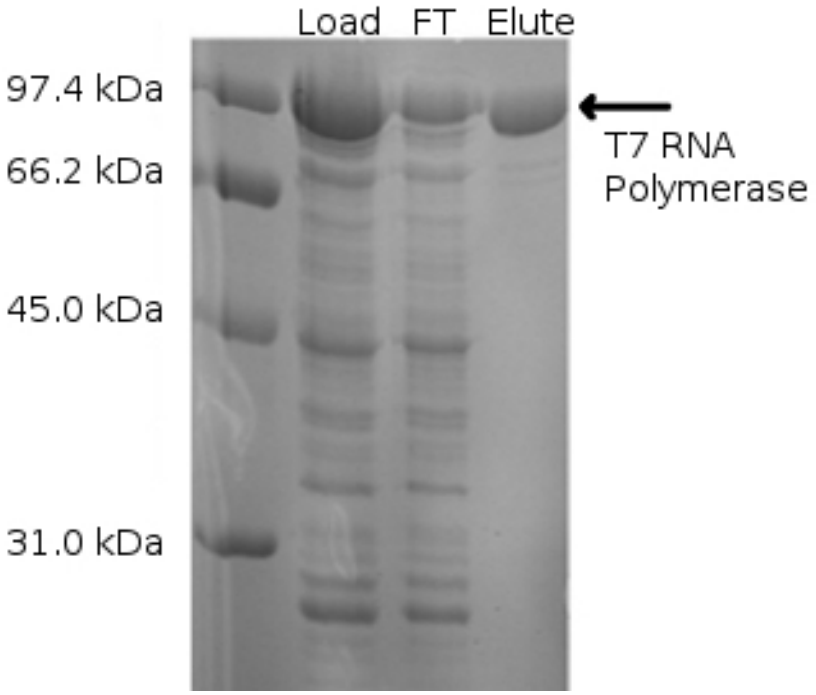

Figure 4.2. A 12% SDS-PAGE gel showing the successful purification of T7-RNA polymerase (80kDa) by Ni-NTA agarose. The polymerase clearly binds to the resin and can be eluted with at greater than 99% purity.

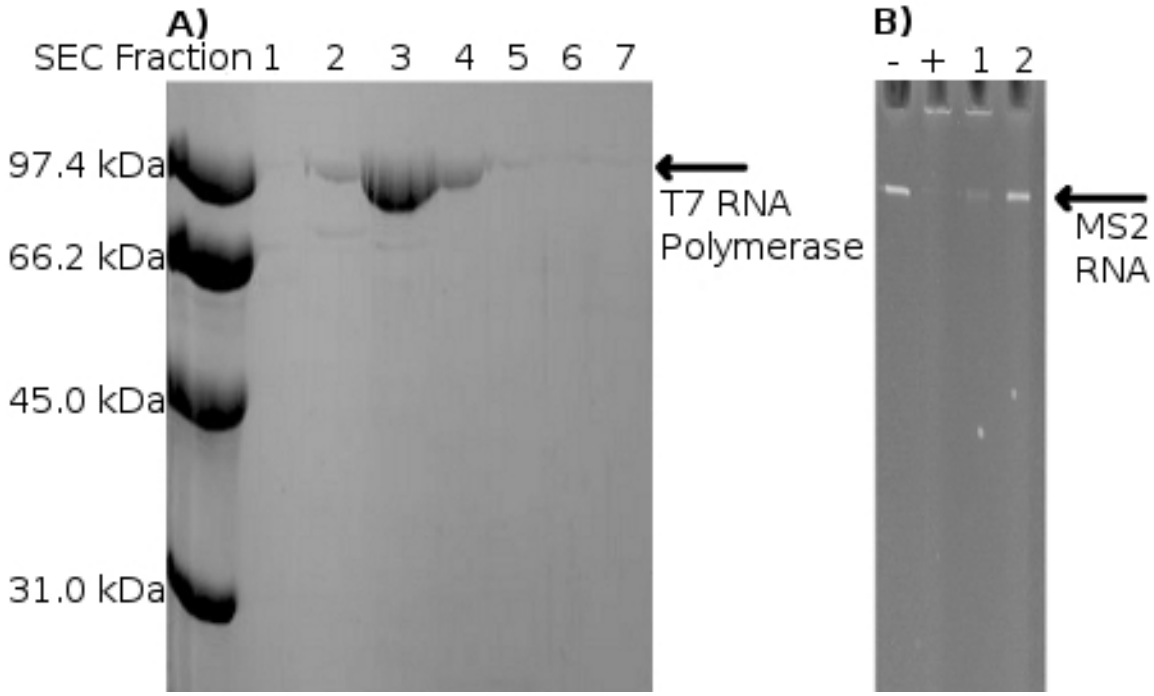

Figure 4.3. A) A 15% SDS-PAGE gel of the fractions collected from the SEC75 column after applying the T7-Polymerase. The polymerase is present in fractions 2-4 and migrates with the expected molecular weight (80kDa). B) An ethidium bromide stained 15% Urea-RNA PAGE gel confirming that the Affi-gel blue gel successfully removes all RNase contamination. Lanes 1 and 2 are controls (-/+ for RNase), lanes 3 and 4 are the T7-polymerase before and after exposure to Affi-gel blue gel.

4.3 Generating guide sRNA for binding experiments

4.3.1 PCR amplification of sR1 DNA template

PCR amplification was used to generate the large quantities of template DNAs required for *in vitro* transcription of guide sRNAs. As illustrated in Figure 4.4 below, the PCR reactions successfully generated DNA templates (A) that were free of RNase contamination (B).

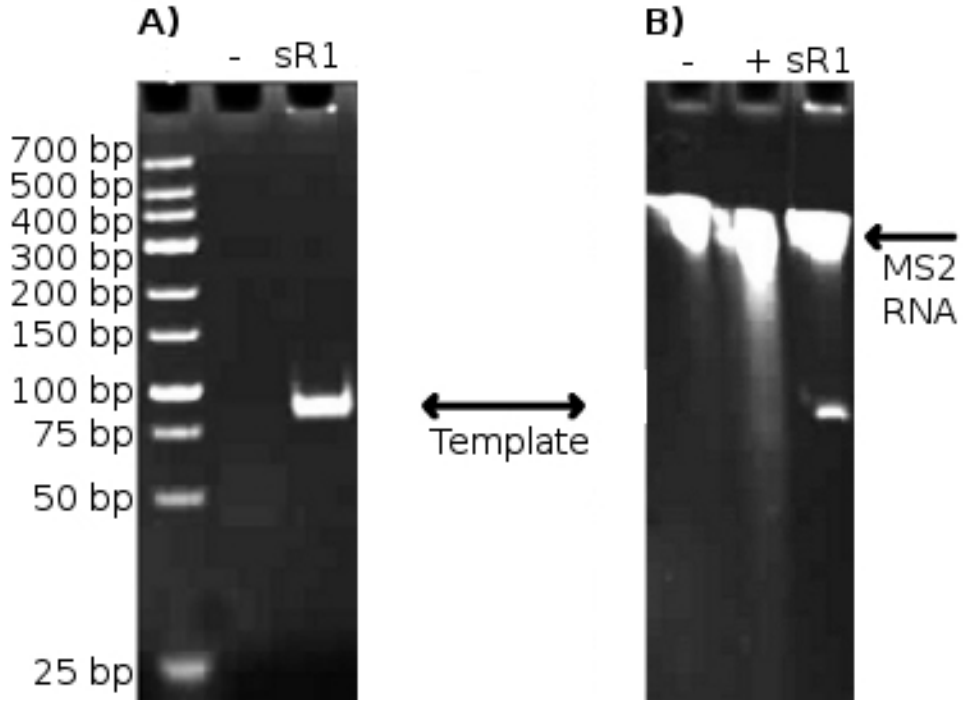

Figure 4.4. Ethidium bromide stained 15% Urea-RNA PAGE gels A) PCR amplification of sR1 was clearly successful (expected size is 83nt), producing large quantities of template. B) RNase tests of the DNA templates confirm that the template is free of RNase contamination.

4.3.2 Production and purification of sR1

Bi partite sR1 sRNA has proven to be a useful model for guide sRNAs, exhibiting most of the features of canonical archaeal sRNAs (Omer *et al.* 2006). This RNA is a representative of the single guide subfamily of box C/D sRNAs and has been shown to direct methylation of 16S rRNA *in vivo* and *in vitro* (Omer *et al.* 2002). Using the *in vitro* transcription techniques outlined in chapter 2, large quantities (1mL of greater than 150μM) of sR1 sRNA were successfully produced. While this is a very large amount of RNA for most experiments, ITC assays require significantly larger amounts of sample. The RNA can be partially recovered (~40%) following the ITC experiments, but a purification procedure is required to remove all L7ae before re-use. Upon successful sR1 purification from the DNA template and transcription components (DNase treatment

followed by ethanol precipitation), the RNA was confirmed to be stable long term (24 hours) at 37°C (Figure 4.5). RNA samples appear as thick bands on Urea RNA-PAGE gels (excessive loads to determine purity), but appear as thin single bands in native PAGE gels (Figure 4.6). Additionally, small variations in the length of the RNA fragments may result when the polymerase "falls off" the end of the DNA template sequence at different nucleotides during transcription (Helm *et al.* 1999). This is not likely to be a concern for binding experiments because the box C/D and C'/D' regions are not located at the ends of the RNA sequence (recall Figure 1.2).

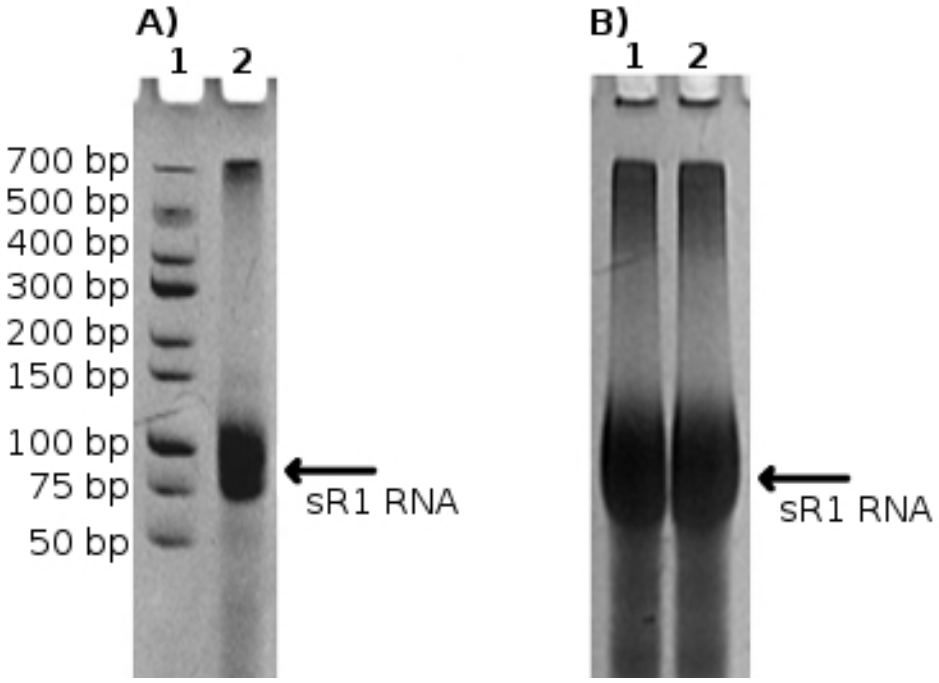

Figure 4.5. RNA transcription reactions visualized on an ethidium bromide stained 15% Urea RNA-PAGE gel illustrating successful transcription (A) and long term RNA stability (>24 hours) (B).

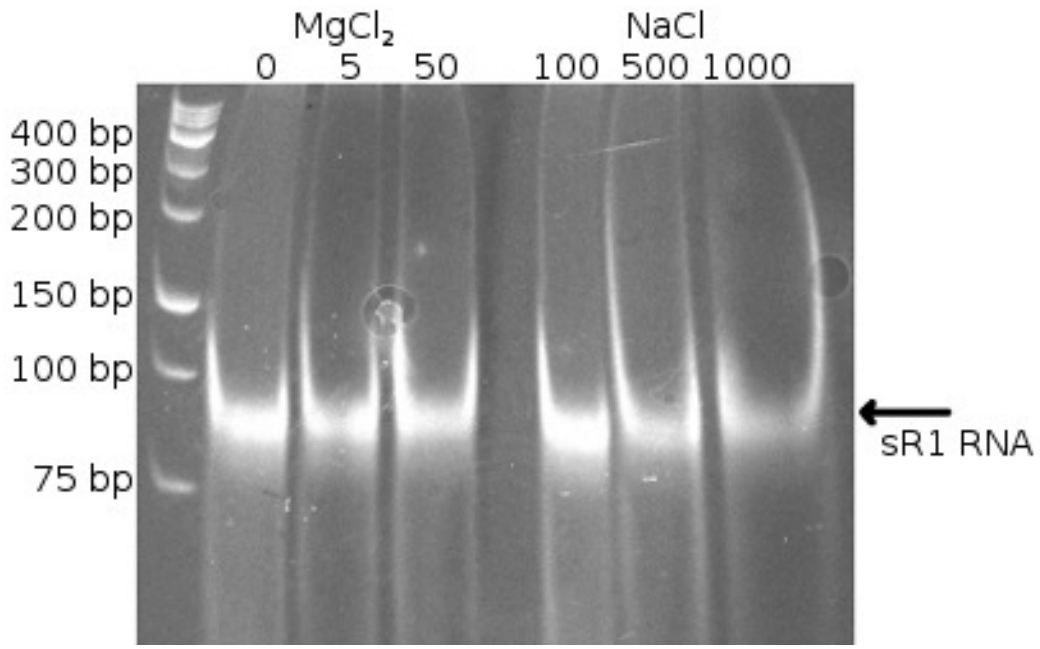

Figure 4.6. Native PAGE gels showing sR1 is monodisperse in a variety of buffers. The effects of $MgCl_2$ were tested with 10mM Tris (pH8) and 250mM NaCl, while the effects of NaCl were tested with 10mM Tris (pH8) and 5mM $MgCl_2$.

4.4 Quantifying the interactions between L7ae and sR1 RNA

4.4.1 Electrophoretic mobility shift assay

The binding interactions between L7ae and sR1 were detected at room temperature by electrophoretic mobility shift assay (Figure 4.7 below). As the ratio of L7ae to RNA increases, the sR1 band shifts to a higher apparent molecular weight. The non-shifted sR1 band intensity was calculated using ImageJ software, and plotted as seen in Figure 4.8. The shifted bands in the 0.4/0.8 (~450 bp) and 1.6/3.2 (>700 bp) molar ratios show different apparent molecular weights, possibly due to a second L7ae binding to the bi-partite sR1. The additional increase in apparent molecular weight at a 4.8 molar ratio may be due to non-specific binding. Fitting the data with a sigmoidal function (Equation 4.1 below) yields a dissociation constant (K_d) of 38.2μM. This may seem high; however, *in vivo* box C/D sRNPs tend to be localized, increasing the effective

concentration. While there are relatively few molar ratios investigated in this experiment, a clear shift can be seen and provides the necessary starting point for a full analysis by ITC.

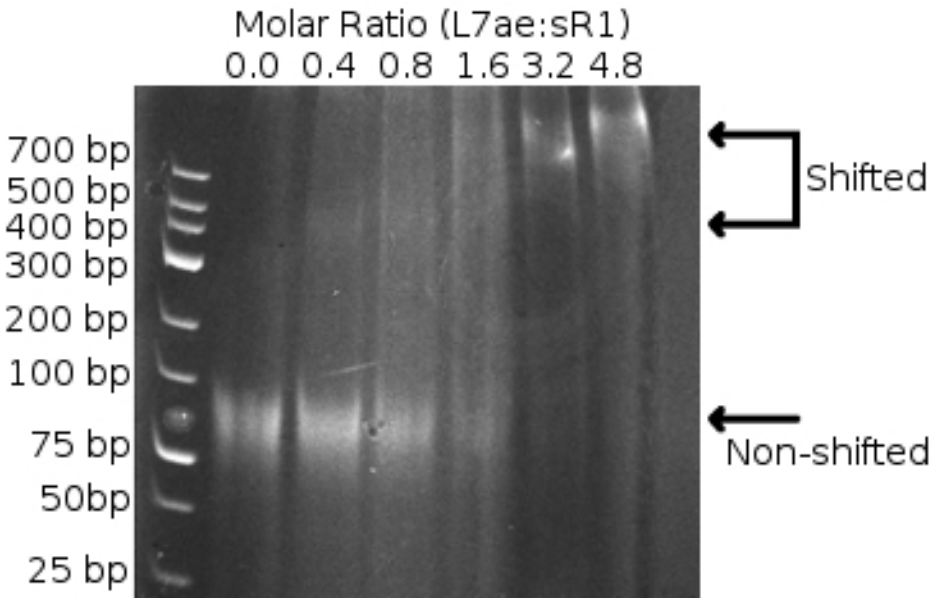

Figure 4.7. An ethidium bromide stained 18% native PAGE gel showing the change in sR1 migration rate in the presence of increasing amounts of L7ae. Initially, all the sR1 migrates as expected (83bp), but upon addition of L7ae the sR1 shifts to a higher apparent molecular weight (near top of gel).

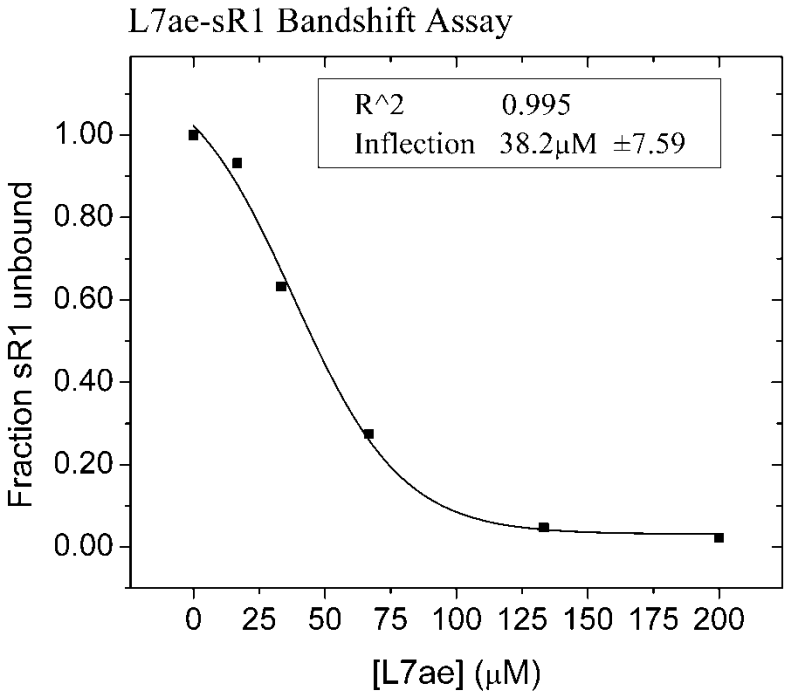

Figure 4.8. Plotted band intensity (unbound sR1) determined from Figure 4.7 with ImageJ. This data can be fit with a sigmoidal function, yielding a K_d of 38.2 $\pm$ 7.56 μM.

$$y = \frac{A_1 - A_2}{1 + e^{(x - x_0)/dx}} + A_2$$

Equation 4.1. The Boltzmann function for producing a sigmoidal curve where A_1 is the initial absorbance, A_2 is the final absorbance, x_0 is the midpoint between A_1 and A_2 and dx is the slope.

4.4.2 Isothermal titration calorimetry (ITC)

ITC is a versatile technique that can be used to study biological interactions in solution. This type of experiment is performed under a constant pressure and a varying volume and records measures the power required to maintain the sample cell at the same temperature as the reference cell. Consequently, the samples are slowly diluted during mixing. ITC can be used to determine binding constants for the L7ae-sR1 interaction (enthalpy (ΔH), association constant (K_a) and stoichiometry (n)), however controls must

be run to ensure these mixing and dilution effects do not produce a significant signal. ITC data was collected at four different temperatures (40^{o}C, 50^{o}C, 55^{o}C and 60^{o}C). The reason for varying temperature is twofold: (1) Additional information for the binding interactions can be obtained (eg. ΔG^{o}, ΔS^{o}, ΔH^{o}) and (2) *S. solfataricus* is a hyperthermophile and temperature may affect the stability of L7ae and RNA.

4.4.2.1 ITC Controls

In order to correct ITC data for any mixing or dilution effects, each component must first be examined individually. Figure 4.9 below shows that titrating buffer into buffer (A), buffer into RNA (B), and L7ae into buffer (C) does not produce a significant signal. Panel D shows that the RNA is not degraded during the titration and can be recovered after the ITC experiment (note that the RNA gets diluted approximately 18% during the complete titration resulting in the lower band intensity in the post lane). Additionally, sRNA titrates were always heated to 75^{o}C and slowly cooled to the chosen experimental temperature to ensure a conformationally consistent (homogeneous) RNA sample.

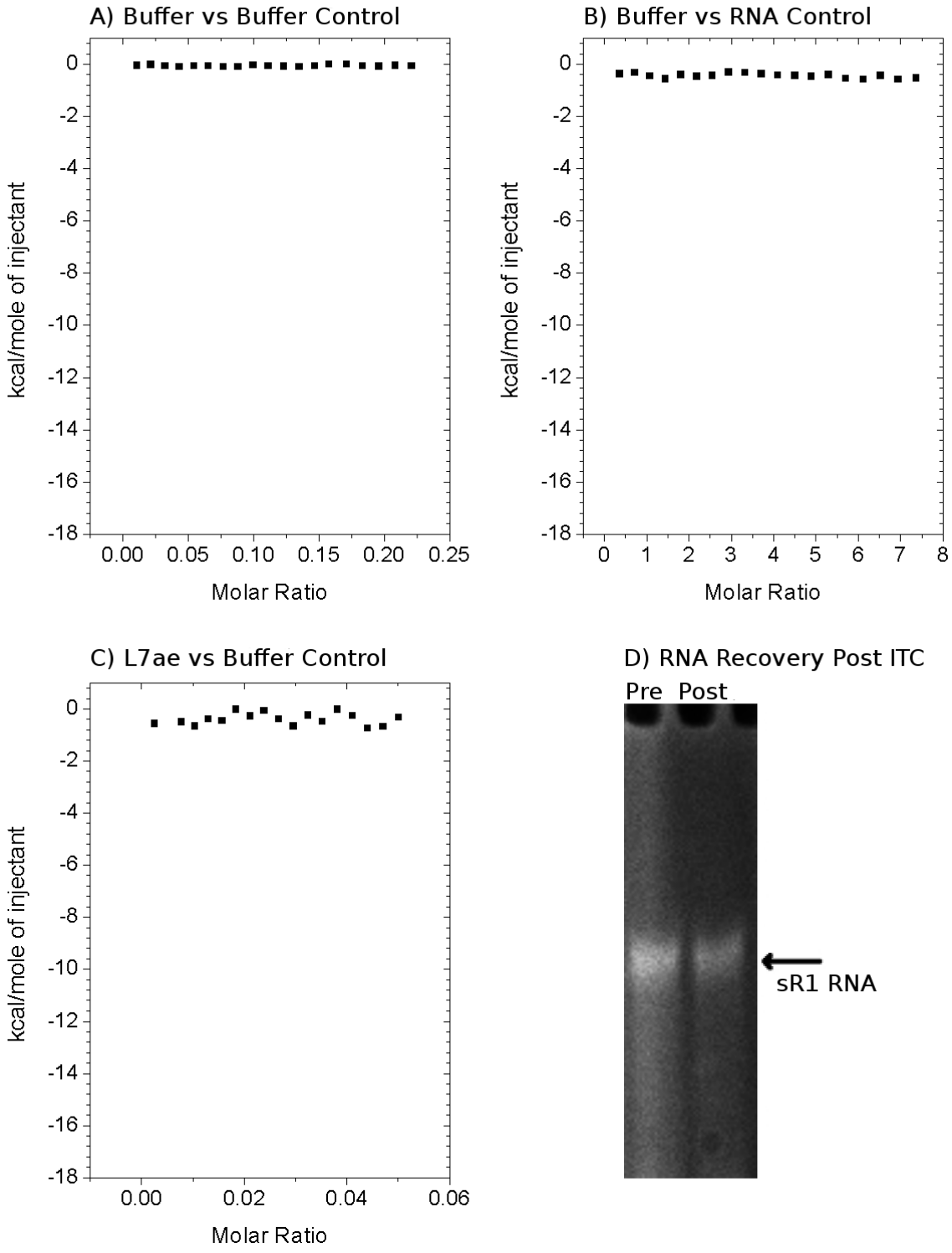

Figure 4.9. ITC experimental controls showing buffer injected into buffer (A), buffer injected into sR1 RNA (B), L7ae injected into Buffer (C), and diluted RNA can be recovered after the experiment (D). The y-axis of all titrations were scaled to that required by the largest signal change.

4.4.2.2 Titrating sR1 with L7ae

The MicroCal™ ITC has a 0.1μcal sensitivity limit and it is recommended that each injection generate an integrated area of greater than 3μcal to minimize error values (MicroCal 2002). ITC studies titrating L7ae into bipartite sR1 RNA were started at 1μM RNA, but yielded little to no signal above the background noise. Increasing the concentration to 15μM yielded a detectable signal but the errors associated with the binding parameters were too large to be usable (errors were same magnitude as the calculated values). While it makes sense to continue increasing the RNA concentration, higher concentrations also increase the chance of forming non-specific interactions (eg. intermolecular RNA interactions). A compromise between the signal strength and RNA sample required was found at 30μM. These titration experiments generated curves of sufficient quality for calculating binding constants. Figure 4.10 below is a representative curve for the data collected during the ITC experiments, and Figure 4.11 illustrates the data collected and processed after titration experiments in buffer S at 40°C, 50°C, 55°C and 60°C. During processing, the data was fit with a single set of identical binding sites model provided by MicoCal™ for use with their ITC equipment (Equation 4.2 below). The resulting data was plotted and a y-axis scale sufficient for the largest signal change was imposed on all data sets.

$$Q = \frac{nM_t \Delta H V_o}{2}\left[1 + \frac{X_t}{nM_t} + \frac{1}{nKM_t} - \sqrt{\left(1 + \frac{X_t}{nM_t} + \frac{1}{nKM_t}\right)^2 - \frac{4X_t}{nM_t}}\right]$$

Equation 4.2. The "single set of identical binding sites" model provided by MicroCal™ for determining thermodynamic parameters from collected ITC data. In this equation Q is the total heat content of the solution, n is number of binding sites, M_t is bulk concentration of macromolecule (RNA), ΔH is the molar heat of ligand binding, V_o is the working volume of the ITC sample cell, X_t is the bulk ligand concentration (L7ae), and K is the association constant.

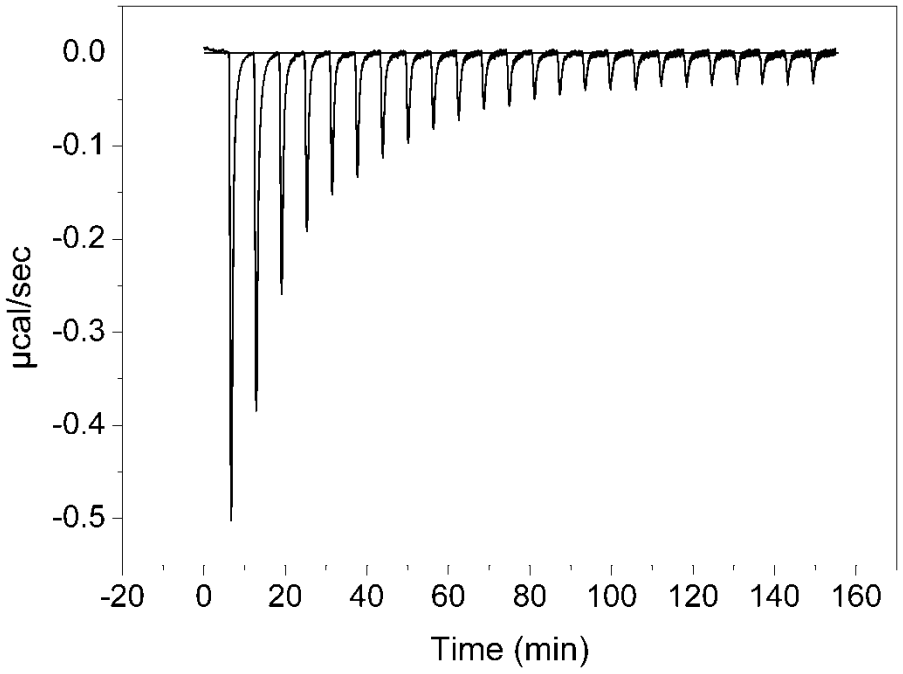

Figure 4.10. A representative plot showing the data collected during an ITC experiment. In this experiment, 30µM sR1 RNA was titrated with 240µM L7ae (10µL injections) in buffer S at 40°C.

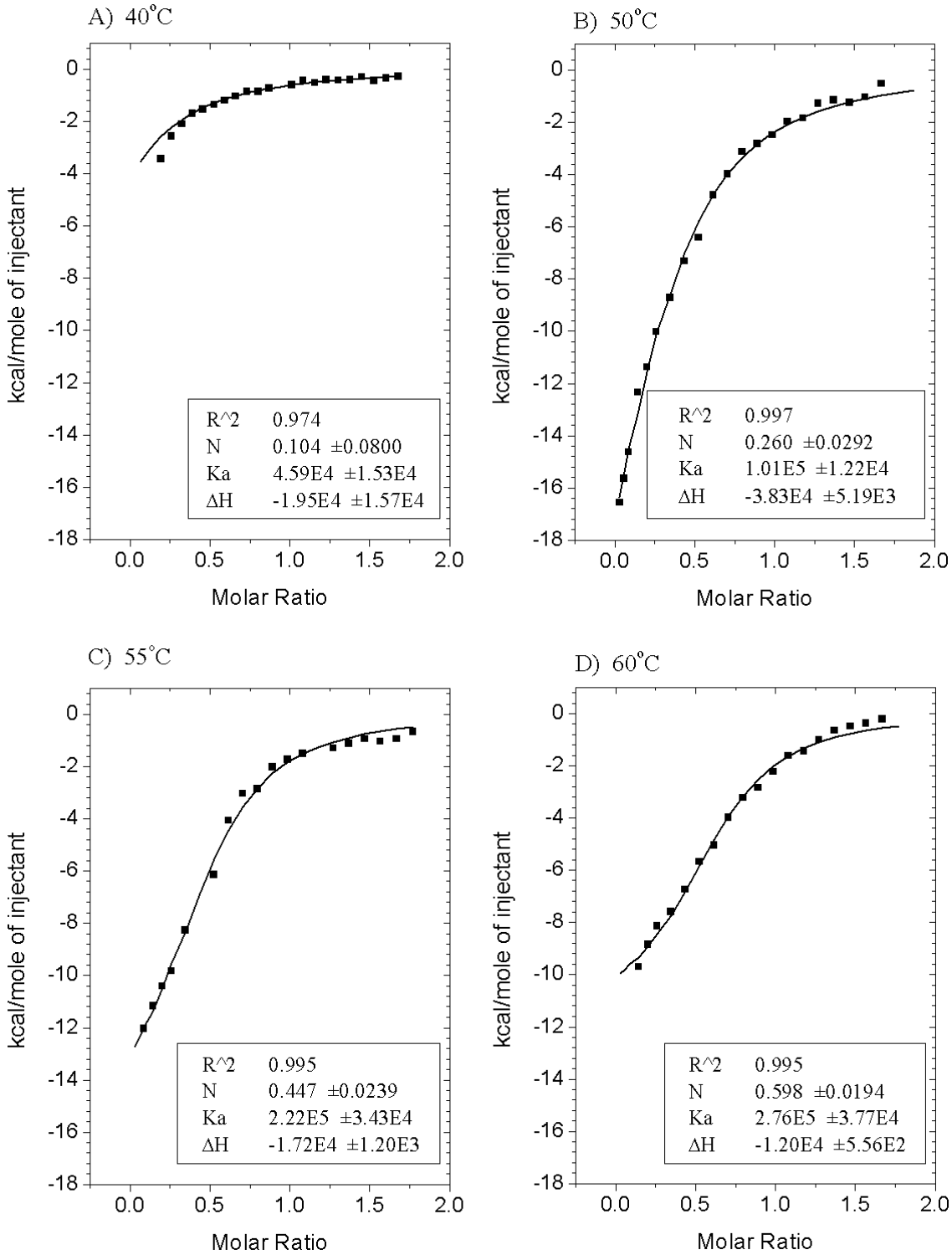

Figure 4.11. ITC experiments at four temperatures (40°C, 50°C, 55°C, and 60°C) in buffer S. The data was scaled using the buffer controls and fit using a single set of identical binding sites model.

Table 4.1. Isotherm data collected in 10mM Tris (pH8), 250mM NaCl, 5mM $MgCl_2$.

Temperature (°C)	Stoichiometry (L7::sR1)	K_d (μM)	ΔH (kcal/mole)
40	0.104 ± 0.0800	21.7 ± 6.05	-19.5 ± 15.7
50	0.260 ± 0.0292	9.90 ± 1.20	-38.3 ± 5.19
55	0.447 ± 0.0239	4.50 ± 0.695	-17.2 ± 1.20
60	0.598 ± 0.0194	3.62 ± 0.494	-12.0 ± 0.556

As seen in Table 4.1 above, the stoichiometry, binding affinity (K_d) and ΔH all appear to have a dependence on temperature (note that the ΔH outside the trend occurs at the lowest stoichiometry and signal strength). The changing stoichiometry is particularly odd because native PAGE gels show the sample to be conformationally homogeneous and since sR1 has two L7ae binding sites the binding stoichiometry should approach 2:1 upon saturation. From the stoichiometry data collected between 40°C and 60°C it was expected that the trend would continue and increasing the temperature would further increase the stoichiometry, however this was not the case. Titrating sR1 RNA with L7ae at 70°C (still below the 87°C optimal growth temperature for *S. solfataricus*) yields no detectable binding interaction. L7ae samples precipitated at temperatures above 75°C, so higher temperature ITC experiments were not performed.

4.3 sR1 RNA T_m data

sR1 heat capacity and melting curves were generated to investigate changes in the RNA sample that would prevent L7ae binding. The experimental melting temperature for sR1 RNA was determined by monitoring the hyperchromatic shift that occurs as nucleic acids melt. The 260nm absorbance (A_{260}) of sR1 RNA was measured in 1.0°C increments between 25°C and 85°C and plotted in Figure 4.12. Applying a sigmoidal fitting curve (Equation 4.1) to the data collected yields an experimental T_m of 74.7 ± 0.566°C. Since this temperature is below the optimal growth temperature of *S. solfataricus*, an additional theoretical heat capacity plot was simulated using the

DINAMelt server (Markham and Zuker 2005) to confirm T_m. This program uses RNA sequences to predict secondary structures and calculate a theoretical heat capacity for the molecule. sR1 heat capacities were calculated from 0°C to 100°C in 0.5°C increment and plotted in Figure 4.13. From the resulting curve the maximum heat capacity (suggesting a melting event) is determined to be 72.5°C. The predicted theoretical melting temperature (72.5°C) agrees well with the calculated experimental data (74.7°C) and together suggests that the sR1 sample is no longer exhibiting the k-turn structure required for L7ae binding at 70°C.

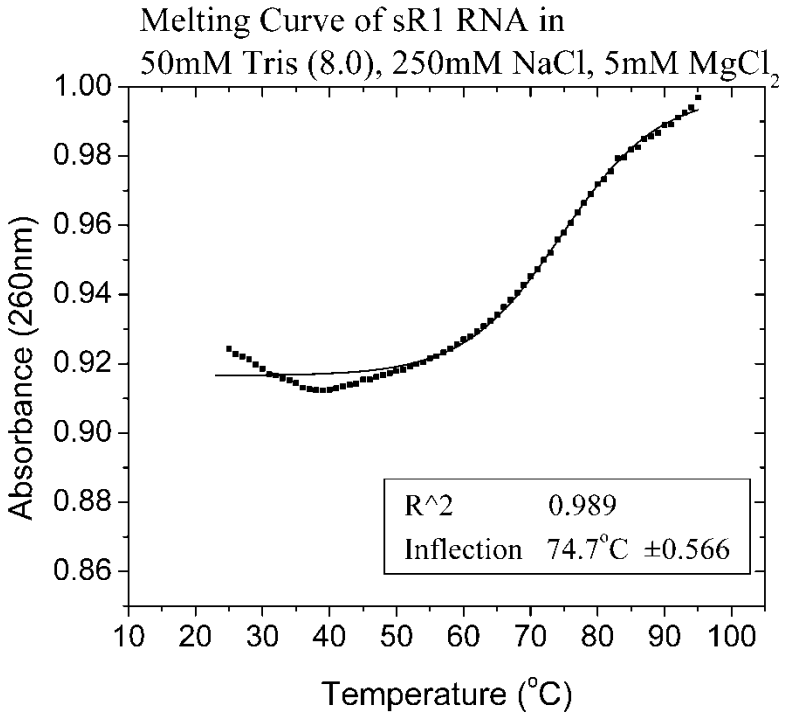

Figure 4.12. An experimental melting curve for 30μM sR1 RNA. UV absorbance was examined in 1.0°C increments and yielded a melting temperature of 74.7°C.

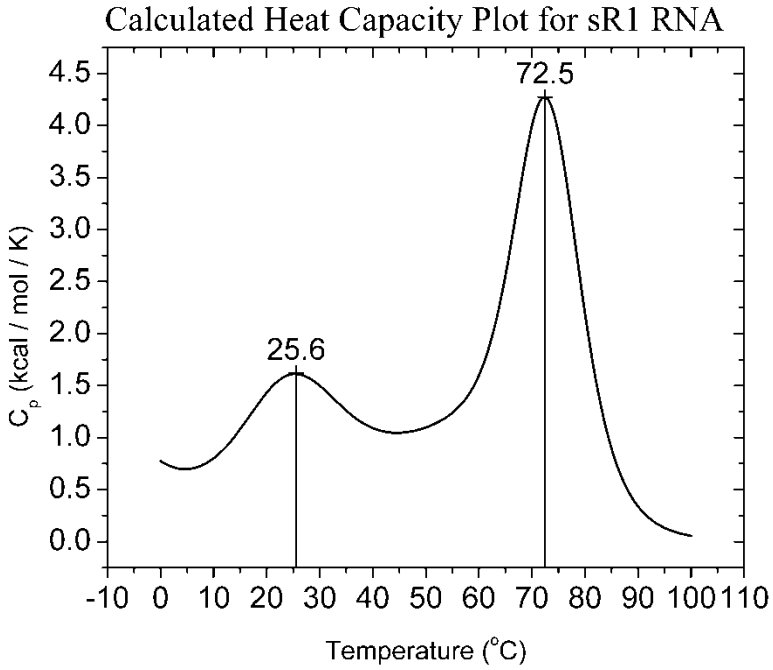

Figure 4.13. A theoretical heat capacity profile for sR1 RNA calculated using the DINAMelt server. Heat capacities were calculated in 0.5°C increments between 0°C and 100°C. From this plot, the melting temperature is found to be 72.5°C with a second event occurring at 25.6°C.

4.4 Measurement of L7ae binding to RNA in alternative buffer conditions

RNA structure can be very sensitive to salt concentration and identity (reviewed in Chen 2008) and Goody *et al.* (2004) shows that both magnesium and sodium chloride concentrations affect the formation of a k-turn structure in sR8. In order to assess the effect of different salts, ITC experiments were carried out in the presence of lower Mg^{2+} concentrations and in the presence of $(NH_4)_2SO_4$. ITC experiments were set up at 50°C and 55°C containing half the magnesium concentration (buffer T) and the resulting data curves are shown in Figure 4.14.

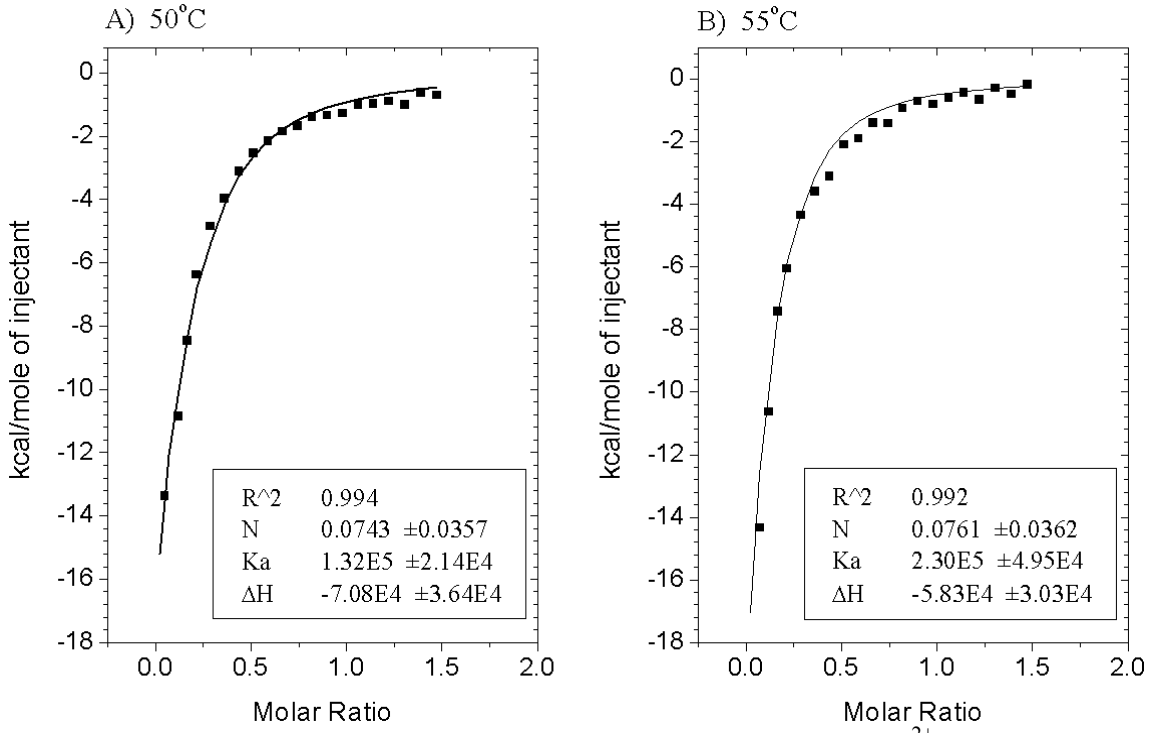

Figure 4.14. ITC experiments at both 50°C and 55°C with reduced Mg^{2+} (buffer T). The data was processed and fit using a single set of identical binding sites model.

Table 4.2. Isotherm data collected in 10mM Tris (pH8), 250mM NaCl, 2.5mM $MgCl_2$.

Temperature (°C)	Stoichiometry (L7::sR1)	K_d (μM)	ΔH (kcal/mole)
50	0.0743 ± 0.0357	7.58 ± 1.23	-70.8 ± 36.4
55	0.0761 ± 0.0362	4.35 ± 0.936	-58.3 ± 30.3

Table 4.2 above summarizes the calculated binding parameters in 2.5mM Mg^{2+}. The determined thermodynamic parameters follow the same trends as seen in Table 4.1, but at a smaller scale. The reduced magnesium does not appear to impact the binding affinity (K_d) significantly, however it does decrease the binding stoichiometry at the equivalent temperatures.

To further investigate the effects of buffer composition, the NaCl was substituted with $(NH_4)_2SO_4$ of approximately equal ionic strength (buffer U). The ITC data was

collected and processed as described above for this buffer system at both 50°C and 55°C and is shown in Figure 4.15.

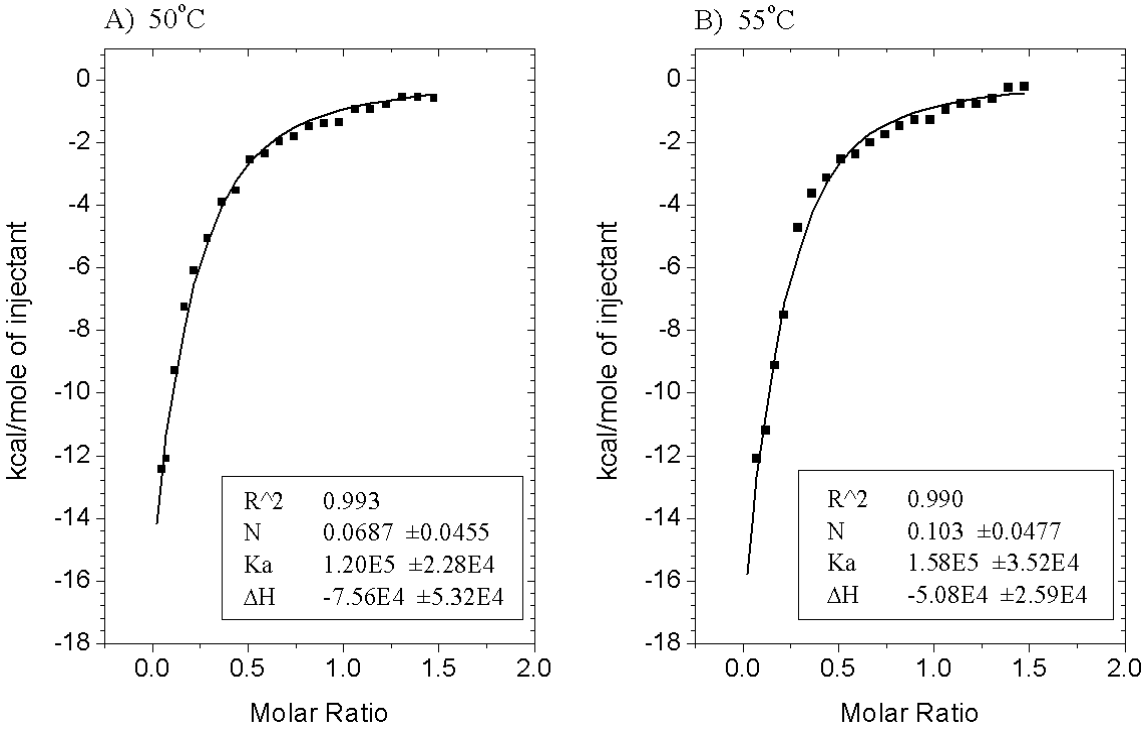

Figure 4.15. ITC experiments at both 50°C and 55°C with NaCl substituted with equal ionic strength $(NH_4)_2SO_4$ (buffer U). The data was processed and fit using a single set of identical binding sites model.

Table 4.3. Isotherm data collected in 10mM Tris (pH8), 83mM $(NH_4)_2SO_4$, 5mM $MgCl_2$.

Temperature (°C)	Stoichiometry (L7::sR1)	K_d (μM)	ΔH (kcal/mole)
50	0.0687 ± 0.0455	13.2 ± 2.48	-75.6 ± 53.2
55	0.103 ± 0.0477	6.33 ± 1.41	-50.8 ± 25.9

The calculated binding parameters summarized in Table 4.3 above follow the same trends seen previously, however the binding affinity and stoichiometry is lower than determined using the NaCl buffer systems.

4.5 Comparison of sR8 to sR1 RNA

The sR1 RNA samples appear to be monodisperse but the stoichiometry of binding suggests that it may not be monodisperse in a k-turn conformation. A second sRNA (sR8) was *in vitro* transcribed, purified and analyzed for stability as described previously. This sample was then compared to sR1 using Urea RNA PAGE and Native RNA PAGE. In the denaturing Urea gel (Figure 4.16a), the RNA is forced to be linear and the two samples appear similar in apparent molecular weight. However, if the samples are not denatured (Figure 4.16b) they do not migrate at the same speed. The faster migrating doublet bands for sR8 suggest secondary structures exist, decreasing the effective length of the molecule and allowing it to migrate faster. While multiple RNA conformations are problematic for ITC experiments, this does confirm that sR8 and sR8 behave differently under the same conditions.

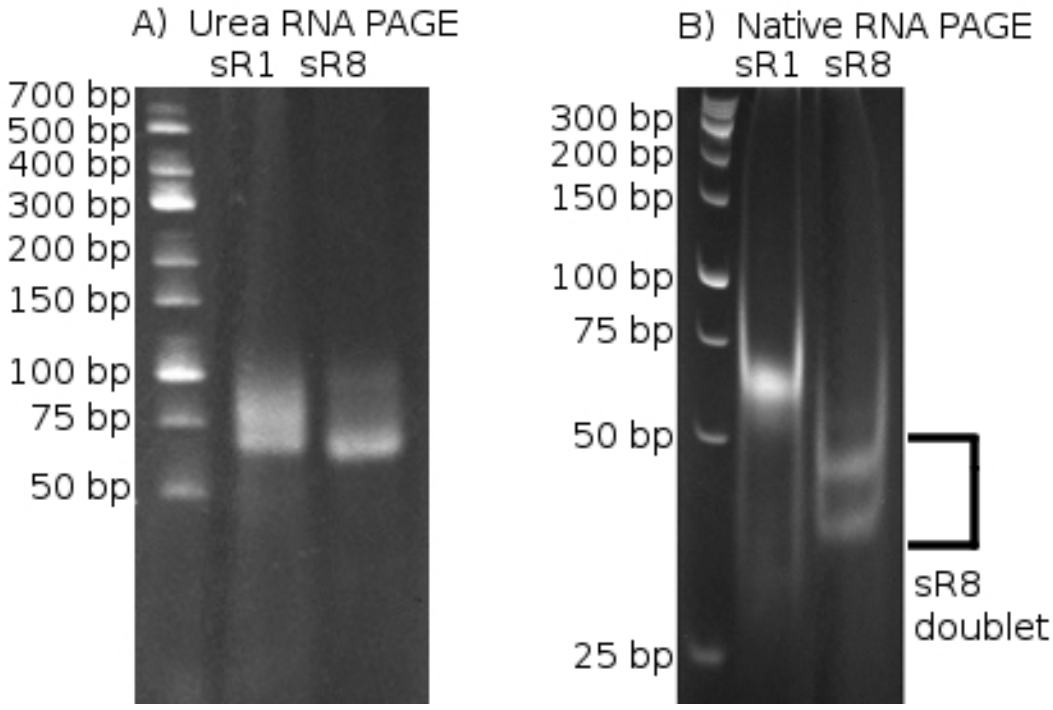

Figure 4.16. Urea (A) and Native (B) RNA PAGE gels comparing the migration rates of sR1 and sR8. Both RNA samples migrate at similar rates when denatured (urea), but sR8 migrates faster than sR1 (and as a doublet) when non-denatured.

Figure 4.16 above suggests sR8 has different structural properties than sR1 and will generate different ITC data curves. An ITC experiment was run in buffer S at 50^{o}C (the same parameters as used in 4.4.3 above), however no binding interaction could be detected under these conditions. This suggests that there are some conformational differences between the two RNA samples and that these differences are affecting the binding interactions.

4.6 Discussion

Sample homogeneity is essential for ITC, as the presence of multiple conformations makes it nearly impossible to analyze and interpret ITC data (Salim and Feig 2009). One of the most common ways to determine RNA monodispersity is Native RNA PAGE (Bhattacharyya *et al.* 1990). When running the sR1 *in vitro* transcription

reactions on this type of gel only a single RNA band can be seen, suggesting a conformationally homogeneous sample is obtained. These samples were then utilized to run a series of ITC experiments at various temperatures. Upon analyzing the collected data, we found that it could be successfully curve fit with the "single set of identical binding sites" model provided by MicroCal™ and the determined dissociation constants and enthalpies were not unreasonably low or high. The curve fitting did however yield an unexpected trend across the temperature range examined. We found that L7ae could not bind to all the calculated binding sites, yielding a stoichiometry much lower than the expected two L7ae per RNA (Bachellerie *et al.* 1995; Tran *et al.* 2003). The calculated stoichiometry displays temperature dependence, with the higher temperatures yielding higher calculated stoichiometries. Notably, the dissociation constant obtained from the preliminary binding assays also fits this trend reasonably well, generating the highest K_d at the lowest temperature. This information suggests that more L7ae binding sites are becoming available and potentially a larger portion of the RNA sample is adopting the k-turn conformation. Using the absorbance at 260/280nm, the L7ae samples were confirmed to be free of RNA, suggesting that the RNA is the component impacting the stoichiometry.

Work by Goody *et al.* (2004) suggests that for sR6 and sR8 an equilibrium can exist between the k-turn and k-turn lacking structures depending on buffer composition. The presence of an equilibrium for k-turn formation presents a problem for ITC data analysis because the signal detected is then a combination of heat evolved when forming the kink-turn followed by the heat evolved when L7ae binds to the consensus sequence and it is difficult to differentiate the two. While varying the temperature to allow the

thermodynamic parameters under standard conditions to be calculated, we found the stoichiometry displays a temperature dependence. A maximum experimental temperature was reached at 70°C, where binding interactions could no longer be detected by ITC. While this is below the optimum growth temperature for *S. solfataricus* (87°C), this oddity has been identified previously. Wilson *et al.* (1990) demonstrated that the DNA binding protein HU from *Bacillus caldolyticus* and *Bacillus stearothermophilus* both have a melting temperature below the organism's optimal growth temperature. At this time, we do not yet know all the other factors which may contribute to thermostability *in vivo* (Ghaemmaghami and Oas 2001).

When sR8 guide sRNA is separated by Native RNA PAGE, a clear doublet band is visible. Additionally, the sample runs as a monomer in denaturing Urea RNA PAGE, suggesting the doublet represents a conformational polydispersity rather than species polydispersity. When sR1 and sR8 are compared on Native RNA PAGE gels we see that both sR8 doublet bands migrate faster than sR1. The difference in apparent molecular weight between the samples suggests that sR8 has a shorter effective length (eg. more secondary structures), allowing it to migrate faster. It also suggests that the sR1 samples exhibits a predominantly unfolded RNA conformation. Interestingly, ITC experiments using sR8 ITC show no binding interactions under the conditions the sR1 data was obtained. It is likely that the data obtained for sR1 actually represents a two step event. The first step would be the formation of a k-turn and the second is L7ae binding to the k-turn. In this model, the sR8 would generate a smaller signal under the same conditions (resulting in no detectable binding), as it would only include the L7ae binding step.

In 2004, Goody *et al.* showed that salts can strongly impact the formation of a kink-turn conformation. Using sR8, they calculated 50% transition states for k-turn formation to occur at 1mM Mg^{2+} ions and 72mM Na^{+}. The Native RNA PAGE gels and analyzed ITC data suggest that sR1 differs from sR8, and that it does not form a k-turn conformation with buffer conditions above the transition states suggested by Goody *et al*. Titration experiments with decreased magnesium content (2.5mM) showed a significantly lower L7ae-sR1 binding stoichiometry (3.5 fold at 50^{o}C and 5.9 fold at 55^{o}C), but did not significantly impact the binding affinity (neither change is larger than the error in the calculated affinities). This data suggests that sR1 does display magnesium dependence, but not identical to sR8 (Goody *et al.* 2004). The studies by Goody *et al.* (2004) and Gagnon *et al.* (2006) were performed using sR8 RNA, which has less sequence variation in the box C/D and C'/D' consensus sequence than sR1. Two possible explanations for our calculated dissociation constants being approximately 10 fold higher than those reported for sR8 (Gagnon *et al.* 2006) are (1) sR1 has more sequence variation from the box C/D consensus sequence than sR8 and/or (2) the ITC may be detecting RNA conformational changes in addition to the binding interactions.

In addition to changing the concentration of Mg^{2+} ions we examined the affect another salt species would have on the formation of a k-turn. When the 250mM NaCl is substituted with 83mM ammonium sulfate (approximately equal ionic strength), L7ae-sR1 binding stoichiometry is reduced (3.8 fold at 50^{o}C and 4.3 fold at 55^{o}C). As seen with the reduced magnesium, ammonium sulfate appears to also have little to no affect on the binding affinity (again neither change is larger than the error in the calculated affinities). This data again suggests that there is a lower population of sR1 molecules

containing the k-turn conformation. Based on all of the above information we suggest that, the buffer compositions tested are not sufficient for sR1 to adopt a k-turn conformation. L7ae binding to k-turn RNA may be more complex than previously thought, containing equilibrium expression for both a k-turn formation and the subsequent binding of L7ae to the formed k-turn.

Buurma and Haq (2007) suggest that if a complex equilibria exists a competitive inhibitor fitting model may be able to fit the data provided (1) the difference in the two equilibria are between two and six orders of magnitude, (2) the inhibitor exerts only a modest effect on the heat evolved, (3) enthalpies of interactions should be sufficiently different for a heat effect to be observed. In the competitor model, the equilibrium between a free enzyme (available to bind substrate) and the enzyme-inhibitor complex (no substrate binding) represents the equilibrium between a k-turn (available to bind L7ae) and k-turn lacking sR1 molecule (unable to bind L7ae). Applying this model to our data generates a K_d of 0.160μM, much closer to the 0.100-0.200μM reported for sR8 (Gagnon *et al.* 2006). Fitting with this model also increases the stoichiometry to 0.774, a 3 fold increase but still far below the expected value of two L7ae per RNA. While this may suggest this is a superior fitting model, the K_d and ΔH for k-turn formation (used as correction factors) are currently unknown and were allowed to optimize during the curve fitting process. This can cause the extra parameters to absorb some of the error and artificially improve fit quality.

We have shown that the buffer compositions reported to stabilize sR8 in a predominantly k-turn confirmation (Goody *et al.* 2004) are insufficient to do the same for sR1. ITC is shown to be a valuable tool for investigating the interactions between L7ae

and sRNAs, however additional work is still required to obtain either (1) a conformationally homogeneous RNA sample or (2) the correction factors (K_d and ΔH for k-turn formation) necessary to apply the competitive inhibitor fitting model.

Chapter 5: Conclusions and Future Directions

5.1 Overview

RNPs are highly dynamic complexes which can adopt multiple conformations throughout their catalytic cycles (Omer *et al.* 2003). Fully assembled sRNPs must always contain the same protein and RNA components arranged in the same orientations, suggesting that the assembly mechanism is strictly controlled to ensure a functional particle is constructed. One of the most common types of RNA modification is the 2'-*O*-methylation of sRNA (Reichow *et al.* 2007). This process is performed by the box C/D sRNP, which is comprised of three proteins and a guide sRNA (in archaea). Figure 1.4 illustrates the currently accepted model for the assembly of Box C/D sRNPs, incorporating nearly all the current experimental data. The only problem arising from this model is the distance between the two Fibrillarin active sites is too far for Fibrillarin to interact with each target site. Previously, structural studies had only been successful with the individual subunits and assembly intermediates, however very recently low resolution structures of the complete sRNP have emerged.

In this work, subunit interactions within an archaeal box C/D methylation sRNP complex from the archaeon *Sulfolobous solfataricus* have been studied. In particular, the Fibrillarin-Nop5 and L7ae-sRNA assembly intermediates were investigated (and) by pulldown assay and isothermal titration calorimetry (ITC) respectively. From the pulldown assays I have demonstrated that dimeric Fibrillarin is still capable of interacting with Nop5, and have also shown that the k-turn sRNA binding by L7ae can be detected and quantified using ITC.

At the outset of this work two contradicting quaternary structures had been experimentally observed for Fibrillarin from different species. In 2000, Fibrillarin was shown to exist as a homodimer (Wang *et al.* 2000). Subsequent studies illustrate that in the presence of Nop5, a Nop5-Fibrillarin heterodimer is formed rather than the Fibrillarin homodimer seen by previously (Aittaleb *et al.* 2003; Aittaleb *et al.* 2004; Oruganti *et al.* 2007). These Fibrillarin dimers have previously been detected experimentally by ITC, analytical ultracentrifugation and size exclusion chromatography (Burke 2006). While obtaining Fibrillarin is relatively straight forward, Nop5 presents a challenge as it is stably unfolded under all tested buffer conditions. This presents a significant problem for ITC studies, because any signal detected would represent both (1) the folding of Nop5 and (2) the binding of Nop5 to Fibrillarin. Further, Nop5 precipitates at concentrations above 5μM, effectively preventing this type of analysis. Fortunately, while developing methods to purify large quantities of Nop5, it was demonstrated that Nop5 undergoes context dependent folding in the presence of Fibrillarin. Therefore I developed a pulldown assay that was used to analyze the interactions between Fibrillarin and Nop5. In this assay, Fibrillarin and Nop5 are shown to interact (presumably context dependent folding), but more interestingly Fibrillarin can also bind as a dimer. In a very recent article (August 2009) Ye *et al.* obtained the structure of a box C/D sRNP with an RNA substrate analog. This structure positions the Fibrillarins close enough together to form the interactions seen by Wang *et al*. (2000), and Ye *et al*. suggests this model represents the final catalytic sRNP.

Chapter 4 examines the binding interactions between L7ae and sRNA. Previously, the interactions between L7ae and sRNA have been identified by

electrophoretic mobility shift assay (Rozhdestvensky *et al.* 2003) and X-ray crystallography (Moore *et al.* 2004; Suryadi *et al.* 2005). In order to obtain quantitative binding and thermodynamic parameters for this interaction, I optimized an *in vitro* transcription and purification approach for sR1 and sR8 guide sRNAs and designed ITC experiments. This work demonstrates that a binding event between L7ae and sR1 can be detected by ITC, and fit to a single set of identical sites binding model (MicroCal 2002). While the association constant and thermodynamic parameters obtained from these fits are reasonable, the stoichiometry of the interaction is low (suggesting incomplete binding). ITC studies at different temperatures and similar studies with sR8 suggest that the low stoichiometry arises from incomplete k-turn formation under our experimental conditions. This suggests that the L7ae-sRNA binding event may be more complicated than previously thought, possibly consisting of both an RNA restructuring event and a binding event. Further work is needed to optimize the experimental conditions to obtain a predominantly k-turn RNA sample and subsequently identify any differences between the sR1 and sR8 binding interactions at various temperatures.

5.2 Interactions between Nop5 and Fibrillarin

RNPs are highly dynamic structures which can adopt multiple conformations to modulate substrate recognition and catalysis. The box C/D methylation complex is one example of the many essential sRNP complexes in cells that require a strictly conserved quaternary structure to be active. Not only does this methylation complex act on many different target molecules (precursor rRNAs/tRNAs in archaea and precursor rRNAs in eucarya) it must also be able to interact with numerous guide RNAs as well (Gaspin *et al.* 2000; Omer *et al.* 2000; Clouet d'Orval *et al.* 2001; Ziesche *et al.* 2004). Efficient

methylation requires two catalytic copies of the sRNP particle (Nop5, Fibrillarin, and L7ae) per guide RNA joined by the coiled-coil domains of the two Nop5 (Rashid *et al.* 2003; Tran *et al.* 2003). The highly dynamic nature of sRNPs, along with domain rearrangements (Oruganti *et al.* 2007), suggest a mechanism to swing the two Fibrillarins close enough to interact with each other. In fact, the X-ray crystal structure generated by Ye *et al.* (2009) presents a quaternary structure with the two Fibrillarin copies close enough to form the dimer we detect. This work on the interactions between Nop5 and Fibrillarin suggests an additional intermediate complex can be formed (Nop5-aFib-aFib). While the role of Fibrillarin dimerization is not yet fully understood, it is reasonable to suggest that these dimers may aid in locking the fully assembled sRNP in an active conformation.

A complete ITC analysis of the Nop5-Fibrillarin interaction is difficult, requiring either (1) an approach to stabilize Nop5 or (2) a known equilibrium constant for the context dependent folding of Nop5 to allow the competitive inhibitor fitting model to be used. Alternatively, given the sequence variation among different organisms, the Nop5 from another organism may be more stable. It may also be possible to study the Fibrillarin dimer in the fully assembled complex by using FRET along with a different fluorescent label on each of the two Fibrillarins. Finally, by looking at the structure by Wang *et al*. (2000) specific amino acids involved in dimerization can be identified and substituted with cysteines to create disulfide bonds between two Fibrillarins. This would effectively lock aFib in its dimer form for subsequent binding experiments. Information obtained from these experiments would lead to an improved model for the pathway to sRNP assembly.

5.3 L7ae binding to Kink-turn RNA

RNA molecules contain various structural motifs (Shen *et al.* 1995) which are sensitive to concentration and identity (reviewed in Chen 2008). L7ae is a member of the RNA binding family that requires a specific kink-turn motif to be present in guide sRNAs for efficient binding to occur (Klein *et al.* 2001; Omer *et al.* 2003; Goody *et al.* 2004). For initial binding studies buffer conditions were chosen according to Goody *et al.* (2004) to promote a large population of k-turn RNA, however the binding stoichiometries obtained from ITC experiments were lower than expected and were affected by temperature. The unexpected stoichiometry and relatively large signal detected for sR1 suggests that the signal may in fact be a combination of (1) the formation of a characteristic k-kink turn conformation and (2) RNA binding by L7ae. This is supported by Suryadi *et al*. (2005) who previously reported that L7ae could induce structural changes in sR8 RNA, similar to the effects they saw when varying magnesium concentrations. Additionally, a gel comparison of sR1 to sR8 suggests that sR1 is exclusively in a non k-turn conformation, however titrating sR8 (which appears to contain secondary structures) generates only a weak signal. While it is possible that L7ae is undergoing conformational rearrangements that contribute to the observed signal, it is notable that L7ae is nearly identical in the RNA-bound and RNA-free states (Hamma and Ferre-D'Amare 2004; Moore *et al.* 2004; Suryadi *et al.* 2005).

Future analysis of the interactions between L7ae and k-turn RNAs should include a search for buffer conditions which promote sR1 k-turn formation. Alternatively, determining the equilibrium constant for kink-turn formation would allow the competitive inhibitor fitting model to be used. Additional studies are also needed to

analyze the stability of k-turns in each of the box C/D sRNAs. By examining the sequence variations within the box C/D sRNAs, those most likely to form stable k-turn structure can be identified and targeted for future analysis. ITC experiments with these RNA samples can provide a thermodynamic basis for understanding the forces which drive RNA-protein binding interactions within box C/D sRNPs.

5.4 Future directions

As described above, we have provided a bridge between the apparently contradictory evidence regarding interactions between Fibrillarin and Nop5. The Fibrillarin dimer has now been identified in both the euryarchaeotal (*Methanococcus jannaschii*) and crenarchaeotal (*Sulfolobus acidocaldarius*) branches archaea. While this dimer is suggested to stabilize/lock the sRNP in an active conformation, not all archaea contain the extended N-terminal domain necessary to form the dimer (eg. *Archaeoglobus fulgidus* and *Pyrococcus furiosus*). Notably, the N-terminal domains of eucaryotic Fibrillarins are also insufficiently long to form dimer interactions, suggesting that these organisms have an alternative approach to stabilize their catalytic complexes. The above work adds to our current understanding of the subunit interactions within box C/D sRNPs, and provides the basis for a model system that can be used to study the assembly of larger, more complex ribonucleoproteins.

To date, we are unable to generate eucaryotic ribosomes *in vitro*, due in a large part to the complex RNA processing that occurs prior to ribosome assembly. The two most common types of RNA modification are the methylation of 2'-hydroxyls and the conversion of uridine to pseudouridine. If it is possible to perform all the RNA modifications *in vitro*, we would be one step closer to being able to produce eucaryotic

ribosomes *in vitro*. Here, we focused on the characteristics of methylation complexes (box C/D sRNP subunit interactions) to increase our understanding of sRNP assembly and catalysis. Work by Filipowicz (2000) suggests that mRNA methylation patterns can affect the rate of translation. Understanding the molecular mechanism for C/D sRNP assembly/catalysis opens the possibilities for designing guide sequences to methylate any target RNA of interest, and can lead to alternative methods for regulating cellular protein expression levels. Current approaches only allow protein expression to be turned on/off, however being able to alter the mRNA methylation patterns provides a tool for regulating protein expression levels in a more precise manner (eg. decrease but not abolish protein expression).

REFERENCES

Abramoff, M.D., Magelhaes, P.J., and Ram, S.J. 2004. Image processing with ImageJ. *Biophotonics International* **11:** 36-42.

Aittaleb, M., Rashid, R., Chen, Q., Palmer, J.R., Daniels, C.J., and Li, H. 2003. Structure and function of archaeal box C/D sRNP core proteins. *Nat Struct Biol* **10:** 256-263.

Aittaleb, M., Visone, T., Fenley, M.O., and Li, H. 2004. Structural and thermodynamic evidence for a stabilizing role of Nop5p in S-adenosyl-L-methionine binding to fibrillarin. *J Biol Chem* **279:** 41822-41829.

Bachellerie, J.P., Michot, B., Nicoloso, M., Balakin, A., Ni, J., and Fournier, M.J. 1995. Antisense snoRNAs: a family of nucleolar RNAs with long complementarities to rRNA. *Trends Biochem Sci* **20:** 261-264.

Beattie, T.L., Zhou, W., Robinson, M.O., and Harrington, L. 2001. Functional multimerization of the human telomerase reverse transcriptase. *Mol Cell Biol* **21:** 6151-6160.

Bhattacharyya, A., Murchie, A.I., and Lilley, D.M. 1990. RNA bulges and the helical periodicity of double-stranded RNA. *Nature* **343:** 484-487.

Bleichert, F., Gagnon, K.T., Brown, B.A., 2nd, Maxwell, E.S., Leschziner, A.E., Unger, V.M., and Baserga, S.J. 2009. A dimeric structure for archaeal box C/D small ribonucleoproteins. *Science* **325:** 1384-1387.

Bortolin, M.L., Bachellerie, J.P., and Clouet-d'Orval, B. 2003. In vitro RNP assembly and methylation guide activity of an unusual box C/D RNA, cis-acting archaeal pre-tRNA(Trp). *Nucleic Acids Res* **31:** 6524-6535.

Bradford, M.M. 1976. A rapid and sensitive method for the quantitation of microgram quantities of protein utilizing the principle of protein-dye binding. *Anal Biochem* **72:** 248-254.

Brosius, J. 2005. Echoes from the past--are we still in an RNP world? *Cytogenet Genome Res* **110:** 8-24.

Burke, P. 2006. The Oligomeric State of Archaeal Fibrillarin: Implications into the Organization and Function of Essential Box C/D sRNP Particles. In *Biochemistry*, pp. 82. Alberta, Lethbridge.

Burkhard, P., Stetefeld, J., and Strelkov, S.V. 2001. Coiled coils: a highly versatile protein folding motif. *Trends Cell Biol* **11:** 82-88.

Buurma, N.J., and Haq, I. 2007. Advances in the analysis of isothermal titration calorimetry data for ligand-DNA interactions. *Methods* **42:** 162-172.

Chen, S.J. 2008. RNA folding: conformational statistics, folding kinetics, and ion electrostatics. *Annu Rev Biophys* **37:** 197-214.

Cheng, X., and Roberts, R.J. 2001. AdoMet-dependent methylation, DNA methyltransferases and base flipping. *Nucleic Acids Res* **29:** 3784-3795.

Chothia, C., and Janin, J. 1975. Principles of protein-protein recognition. *Nature* **256:** 705-708.

Clouet d'Orval, B., Bortolin, M.L., Gaspin, C., and Bachellerie, J.P. 2001. Box C/D RNA guides for the ribose methylation of archaeal tRNAs. The tRNATrp intron guides the formation of two ribose-methylated nucleosides in the mature tRNATrp. *Nucleic Acids Res* **29:** 4518-4529.

Deng, L., Starostina, N.G., Liu, Z.J., Rose, J.P., Terns, R.M., Terns, M.P., and Wang, B.C. 2004. Structure determination of fibrillarin from the hyperthermophilic archaeon Pyrococcus furiosus. *Biochem Biophys Res Commun* **315:** 726-732.

Dennis, P.P., Omer, A., and Lowe, T. 2001. A guided tour: small RNA function in Archaea. *Mol Microbiol* **40:** 509-519.

Eddy, S.R. 2001. Non-coding RNA genes and the modern RNA world. *Nat Rev Genet* **2:** 919-929.

Eichler, D.C., and Craig, N. 1994. Processing of eukaryotic ribosomal RNA. *Prog Nucleic Acid Res Mol Biol* **49:** 197-239.

Erdmann, V.A., Barciszewska, M.Z., Szymanski, M., Hochberg, A., de Groot, N., and Barciszewski, J. 2001. The non-coding RNAs as riboregulators. *Nucleic Acids Res* **29:** 189-193.

Fallon, A.M., Jinks, C.S., Strycharz, G.D., and Nomura, M. 1979. Regulation of ribosomal protein synthesis in Escherichia coli by selective mRNA inactivation. *Proc Natl Acad Sci U S A* **76:** 3411-3415.

Fatica, A., and Tollervey, D. 2003. Insights into the structure and function of a guide RNP. *Nat Struct Biol* **10:** 237-239.

Fersht, A. 1999. *Structure and Mechanism in Protein Science: A guide to enzyme catalysis and protein folding*. W.H. Freeman and Company, New York.

Filipowicz, W. 2000. Imprinted expression of small nucleolar RNAs in brain: time for RNomics. *Proc Natl Acad Sci U S A* **97:** 14035-14037.

Gagnon, K.T., Zhang, X., Agris, P.F., and Maxwell, E.S. 2006. Assembly of the archaeal box C/D sRNP can occur via alternative pathways and requires temperature-facilitated sRNA remodeling. *J Mol Biol* **362:** 1025-1042.

Galardi, S., Fatica, A., Bachi, A., Scaloni, A., Presutti, C., and Bozzoni, I. 2002. Purified box C/D snoRNPs are able to reproduce site-specific 2'-O-methylation of target RNA in vitro. *Mol Cell Biol* **22:** 6663-6668.

Gaspin, C., Cavaille, J., Erauso, G., and Bachellerie, J.P. 2000. Archaeal homologs of eukaryotic methylation guide small nucleolar RNAs: lessons from the Pyrococcus genomes. *J Mol Biol* **297:** 895-906.

Gasteiger, E., Hoogland, A., Gattiker, S., Duvaud, M.R., and Appel, A. 2005. *Protein identification and analysis tools on the ExPASy server*. Humana Press, Totowa, NJ.

Gautier, T., Berges, T., Tollervey, D., and Hurt, E. 1997. Nucleolar KKE/D repeat proteins Nop56p and Nop58p interact with Nop1p and are required for ribosome biogenesis. *Mol Cell Biol* **17:** 7088-7098.

Ghaemmaghami, S., and Oas, T.G. 2001. Quantitative protein stability measurement in vivo. *Nat Struct Biol* **8:** 879-882.

Goody, T.A., Melcher, S.E., Norman, D.G., and Lilley, D.M. 2004. The kink-turn motif in RNA is dimorphic, and metal ion-dependent. *RNA* **10:** 254-264.

Hamma, T., and Ferre-D'Amare, A.R. 2004. Structure of protein L7Ae bound to a K-turn derived from an archaeal box H/ACA sRNA at 1.8 A resolution. *Structure* **12:** 893-903.

Hardin, J.W., Reyes, F.E., and Batey, R.T. 2009. Analysis of a critical interaction within the archaeal box C/D small ribonucleoprotein complex. *J Biol Chem* **284:** 15317-15324.

Heine, M.A., Rankin, M.L., and DiMario, P.J. 1993. The Gly/Arg-rich (GAR) domain of Xenopus nucleolin facilitates in vitro nucleic acid binding and in vivo nucleolar localization. *Mol Biol Cell* **4:** 1189-1204.

Helm, M., Brule, H., Giege, R., and Florentz, C. 1999. More mistakes by T7 RNA polymerase at the 5' ends of in vitro-transcribed RNAs. *RNA* **5:** 618-621.

Kiss-Laszlo, Z., Henry, Y., Bachellerie, J.P., Caizergues-Ferrer, M., and Kiss, T. 1996. Site-specific ribose methylation of preribosomal RNA: a novel function for small nucleolar RNAs. *Cell* **85:** 1077-1088.

Kiss-Laszlo, Z., Henry, Y., and Kiss, T. 1998. Sequence and structural elements of methylation guide snoRNAs essential for site-specific ribose methylation of pre-rRNA. *EMBO J* **17:** 797-807.

Kiss, T. 2001. Small nucleolar RNA-guided post-transcriptional modification of cellular RNAs. *EMBO J* **20:** 3617-3622.

Kiss, T. 2004. Biogenesis of small nuclear RNPs. *J Cell Sci* **117:** 5949-5951.

Klein, D.J., Schmeing, T.M., Moore, P.B., and Steitz, T.A. 2001. The kink-turn: a new RNA secondary structure motif. *EMBO J* **20:** 4214-4221.

Kohn, W.D., Mant, C.T., and Hodges, R.S. 1997. Alpha-helical protein assembly motifs. *J Biol Chem* **272:** 2583-2586.

Kowalak, J.A., Dalluge, J.J., McCloskey, J.A., and Stetter, K.O. 1994. The role of posttranscriptional modification in stabilization of transfer RNA from hyperthermophiles. *Biochemistry* **33:** 7869-7876.

Lechertier, T., Grob, A., Hernandez-Verdun, D., and Roussel, P. 2009. Fibrillarin and Nop56 interact before being co-assembled in box C/D snoRNPs. *Exp Cell Res* **315:** 928-942.

Liu, B., Ni, J., and Fournier, M.J. 2001. Probing RNA in vivo with methylation guide small nucleolar RNAs. *Methods* **23:** 276-286.

Lowe, T.M., and Eddy, S.R. 1999. A computational screen for methylation guide snoRNAs in yeast. *Science* **283:** 1168-1171.

Markham, N.R., and Zuker, M. 2005. DINAMelt web server for nucleic acid melting prediction. *Nucleic Acids Res* **33:** W577-581.

Martin, J.L., and McMillan, F.M. 2002. SAM (dependent) I AM: the S-adenosylmethionine-dependent methyltransferase fold. *Curr Opin Struct Biol* **12:** 783-793.

Maxwell, E.S., and Fournier, M.J. 1995. The small nucleolar RNAs. *Annu Rev Biochem* **64:** 897-934.

MicroCal. 2002. VP-ITC User Manual.

Moore, T., Zhang, Y., Fenley, M.O., and Li, H. 2004. Molecular basis of box C/D RNA-protein interactions; cocrystal structure of archaeal L7Ae and a box C/D RNA. *Structure* **12:** 807-818.

Nottrott, S., Urlaub, H., and Luhrmann, R. 2002. Hierarchical, clustered protein interactions with U4/U6 snRNA: a biochemical role for U4/U6 proteins. *EMBO J* **21:** 5527-5538.

Ofengand, J. 2002. Ribosomal RNA pseudouridines and pseudouridine synthases. *FEBS Lett* **514:** 17-25.

Omer, A.D., Lowe, T.M., Russell, A.G., Ebhardt, H., Eddy, S.R., and Dennis, P.P. 2000. Homologs of small nucleolar RNAs in Archaea. *Science* **288:** 517-522.

Omer, A.D., Zago, M., Chang, A., and Dennis, P.P. 2006. Probing the structure and function of an archaeal C/D-box methylation guide sRNA. *RNA* **12:** 1708-1720.

Omer, A.D., Ziesche, S., Decatur, W.A., Fournier, M.J., and Dennis, P.P. 2003. RNA-modifying machines in archaea. *Mol Microbiol* **48:** 617-629.

Omer, A.D., Ziesche, S., Ebhardt, H., and Dennis, P.P. 2002. In vitro reconstitution and activity of a C/D box methylation guide ribonucleoprotein complex. *Proc Natl Acad Sci U S A* **99:** 5289-5294.

Oruganti, S., Zhang, Y., Li, H., Robinson, H., Terns, M.P., Terns, R.M., and Yang, W. 2007. Alternative conformations of the archaeal Nop56/58-fibrillarin complex imply flexibility in box C/D RNPs. *J Mol Biol* **371:** 1141-1150.

Rashid, R., Aittaleb, M., Chen, Q., Spiegel, K., Demeler, B., and Li, H. 2003. Functional requirement for symmetric assembly of archaeal box C/D small ribonucleoprotein particles. *J Mol Biol* **333:** 295-306.

Reichow, S.L., Hamma, T., Ferre-D'Amare, A.R., and Varani, G. 2007. The structure and function of small nucleolar ribonucleoproteins. *Nucleic Acids Res* **35:** 1452-1464.

Rozhdestvensky, T.S., Tang, T.H., Tchirkova, I.V., Brosius, J., Bachellerie, J.P., and Huttenhofer, A. 2003. Binding of L7Ae protein to the K-turn of archaeal snoRNAs: a shared RNA binding motif for C/D and H/ACA box snoRNAs in Archaea. *Nucleic Acids Res* **31:** 869-877.

Salim, N.N., and Feig, A.L. 2009. Isothermal titration calorimetry of RNA. *Methods* **47:** 198-205.

Sambrook, J., and Russell, D. 2001. *Molecular Cloning: A laboratory Manual*, Third Edition ed. Cold Spring Harbor Laboratory Press, Cold Spring Harbor, New York.

Shen, L.X., Cai, Z., and Tinoco, I., Jr. 1995. RNA structure at high resolution. *FASEB J* **9:** 1023-1033.

Stoschek, C.M. 1990. Quantitation of Protein. *Methods in Enzymology* **182:** 50-69.

Suryadi, J., Tran, E.J., Maxwell, E.S., and Brown, B.A., 2nd. 2005. The crystal structure of the Methanocaldococcus jannaschii multifunctional L7Ae RNA-binding protein reveals an induced-fit interaction with the box C/D RNAs. *Biochemistry* **44:** 9657-9672.

Tollervey, D., Lehtonen, H., Carmo-Fonseca, M., and Hurt, E.C. 1991. The small nucleolar RNP protein NOP1 (fibrillarin) is required for pre-rRNA processing in yeast. *EMBO J* **10:** 573-583.

Tran, E., Brown, J., and Maxwell, E.S. 2004. Evolutionary origins of the RNA-guided nucleotide-modification complexes: from the primitive translation apparatus? *Trends Biochem Sci* **29:** 343-350.

Tran, E., Zhang, X., Lackey, L., and Maxwell, E.S. 2005. Conserved spacing between the box C/D and C'/D' RNPs of the archaeal box C/D sRNP complex is required for efficient 2'-O-methylation of target RNAs. *RNA* **11:** 285-293.

Tran, E.J., Zhang, X., and Maxwell, E.S. 2003. Efficient RNA 2'-O-methylation requires juxtaposed and symmetrically assembled archaeal box C/D and C'/D' RNPs. *EMBO J* **22:** 3930-3940.

Tycowski, K.T., Smith, C.M., Shu, M.D., and Steitz, J.A. 1996. A small nucleolar RNA requirement for site-specific ribose methylation of rRNA in Xenopus. *Proc Natl Acad Sci U S A* **93:** 14480-14485.

Voet, D., and Voet, J. 2004. *Biochemistry*, 3rd ed. John Wiley and Sons Inc., Hoboken, New Jersey, pp. 1591.

Wang, C., and Meier, U.T. 2004. Architecture and assembly of mammalian H/ACA small nucleolar and telomerase ribonucleoproteins. *EMBO J* **23:** 1857-1867.

Wang, H., Boisvert, D., Kim, K.K., Kim, R., and Kim, S.H. 2000. Crystal structure of a fibrillarin homologue from Methanococcus jannaschii, a hyperthermophile, at 1.6 A resolution. *EMBO J* **19:** 317-323.

Wassarman, K.M., Zhang, A., and Storz, G. 1999. Small RNAs in Escherichia coli. *Trends Microbiol* **7:** 37-45.

Wilson, K.S., Vorgias, C.E., Tanaka, I., White, S.W., and Kimura, M. 1990. The thermostability of DNA-binding protein HU from bacilli. *Protein Eng* **4:** 11-22.

Wu, H., Min, J., Zeng, H., Loppnau, P., Weigelt, J., Sundstrom, M., Arrowsmith, C.H., Edwards, A.M., Bochkarev, A., and Plotnikov, A.N. 2006. Unpublished data, PDB ID 2IPX.

Ye, K., Jia, R., Lin, J., Ju, M., Peng, J., Xu, A., and Zhang, L. 2009. Structural organization of box C/D RNA-guided RNA methyltransferase. *Proc Natl Acad Sci U S A* **106:** 13808-13813.

Zhang, X., Champion, E.A., Tran, E.J., Brown, B.A., 2nd, Baserga, S.J., and Maxwell, E.S. 2006. The coiled-coil domain of the Nop56/58 core protein is dispensable for sRNP assembly but is critical for archaeal box C/D sRNP-guided nucleotide methylation. *RNA* **12:** 1092-1103.

Ziesche, S.M., Omer, A.D., and Dennis, P.P. 2004. RNA-guided nucleotide modification of ribosomal and non-ribosomal RNAs in Archaea. *Mol Microbiol* **54:** 980-993.